TOPICAL REVIEW

Protein Electron Transfer: Is Biology (Thermo)dynamic?

Dmitry V. Matyushov

Department of Physics and Department of Chemistry & Biochemistry, Arizona State University, PO Box 871504, Tempe, AZ 85287-1504

E-mail: dmitrym@asu.edu

Abstract. Simple physical mechanisms are behind the flow of energy in all forms of life. Energy comes to living systems through electrons occupying high-energy states, either from food (respiratory chains) or from light (photosynthesis). This energy is transformed into the cross-membrane proton-motive force that eventually drives all biochemistry of the cell. Life's ability to transfer electrons over large distances with nearly zero loss of free energy is puzzling and has not been accomplished in synthetic systems. The focus of this review is on how this energetic efficiency is realized. General physical mechanisms and interactions that allow proteins to fold into compact water-soluble structures are also responsible for a rugged landscape of energy states and a broad distribution of relaxation times. Specific to a protein as a fluctuating thermal bath is the protein-water interface, which is heterogeneous both dynamically and structurally. The spectrum of interfacial fluctuations is a consequence of protein's elastic flexibility combined with a high density of surface charges polarizing water dipoles into surface nanodomains. Electrostatics is critical to the protein function and the relevant questions are: (i) What is the spectrum of interfacial electrostatic fluctuations? (ii) Does the interfacial biological water produce electrostatic signatures specific to proteins? (iii) How is protein-mediated chemistry affected by electrostatics? These questions connect the fluctuation spectrum to the dynamical control of chemical reactivity, i.e., the dependence of the activation free energy of the reaction on the dynamics of the bath. Ergodicity is often broken in protein-driven reactions and thermodynamic free energies become irrelevant. Continuous ergodicity breaking in a dense spectrum of relaxation times requires using dynamically restricted ensembles to calculate statistical averages. When applied to the calculation of the rates, this formalism leads to the nonergodic activated kinetics, which extends the transition-state theory to dynamically dispersive media. Releasing the grip of thermodynamics in kinetic calculations through nonergodicity provides the mechanism for an efficient optimization between reaction rates and the spectrum of relaxation times of the protein-water thermal bath. Bath dynamics, it appears, play as important role as the free energy in optimizing biology's performance.

Keywords: electron transfer; photosynthesis; protein electrostatics; ergodicity breaking; bioenergetics; non-Arrhenius kinetics; protein-water interface.

PACS numbers: 82.30.Fi, 87.14.ep, 87.15.kr, 82.20.Wt

Submitted to: *J. Phys.: Condens. Matter*

1. Introduction

When encountered with the diversity of life one often wonders if there are general principles of life, similar to general principles of physics underlying the complexity of real physical systems. There is probably no established account of biology's fundamental laws, but, it seems, there is an agreement that at least two general principles are common to the operation of all living organisms on the molecular scale: (1) The storage of genetic information in DNA and (2) The origin of biological energy from the cross-membrane gradient of the proton chemical potential (proton-motive force) [1]. The present review deals with the second general principle and addresses the physical processes leading to the creation of the proton-motive force by living cells. The above list is not meant to be exhaustive. For instance, Monod called the allosteric effect briefly discussed by the end of this review "the second secret of life" [2].

The difference of chemical potential of protons outside (periplasm) and inside (cytoplasm) of the cellular membrane has two components: the direct cross-membrane electrostatic potential and the concentration gradient. They add up to produce ~ 150 meV in the chemical potential difference, which ultimately drives the production of ATP in the ATP-synthase. In order to produce a higher proton concentration in the periplasm, oppositely charged electrons need to be transferred from outside to inside the membrane. Cross-membrane electron transport is realized as hopping conductance of electrons between cofactors located within membrane-bound proteins, often referred to as energy complexes of biology's energy chains [3]. Cofactors are chemical compounds capable of changing their electronic redox state, that is to localize an electron on one of their electronic levels. Each elementary step in this sequence of electron hops occurs as an underbarrier electron tunneling between the initial state of localization on the donor and the final state of localization on the acceptor. This elementary step in the overall hopping conductance, or electron transport, is also known as the electron transfer reaction. It has been much studied in the context of redox chemistry in homogeneous solutions [4, 5] and in relation to heterogeneous electrode reactions of electrochemistry [6]. This review is mostly concerned with the mechanistic principles of individual tunneling events involving protein media, although the time-scales of electron localization on individual cofactors of the chain is an important part of the ergodicity breaking arguments discussed below.

The overall balance of free energy is our main concern in an attempt to understand which parameters of the electron transport chain are optimized for the overall performance. Performance, or efficiency, is understood here as the optimal use of the input chemical potential for the catalytic storage of energy by the enzymes. The problems of the thermodynamic efficiency of the cell or of the electron-transport chain viewed as a heat engine [7] are not considered here. Our main focus is therefore on the mechanistic principles that allow to keep electrons in the high free energy state. From the viewpoint of the free energy balance, the electron transport chain is an input/output device in which the input is realized through high-energy electrons either from reducing

agents of food (mitochondria of eukaryotic cells [1]) or from light (bacterial and plant photosynthesis [8]). The output of the chain is the catalytic conversion of the input energy into the energy of chemical bonds, which, in the case of eukaryotic mitochondria, is the reaction combining four electrons, four protons from the cytoplasm and an oxygen molecule to produce water. Between the input and output lies the electron transport chain composed of a number of cofactors ($\sim$ 22 for mitochondria [3]) between which electrons tunnel.

Living cells have been optimized to survive on a relatively low input free energy, $\sim 1.1-1.4$ eV [3]. This free energy has to support the unidirectional transfer of electrons along the chain. The mechanistic challenge encountered by this design is that competing and potentially harmful oxidation reactions need to be prevented and, additionally, the turn-over of the electron-transport chain should not be slower than the catalytic reaction on the cytoplasmic side of the membrane. Both conditions require lowering the activation barriers of individual hops along the chain. This stipulates, in turn, exergonic reactions (negative reaction free energy). The best condition for electron tunneling is achieved when there is no barrier at all (activationless reaction), which has been proven for several electron-transfer steps at the beginning of the electron transport chain of bacterial photosynthesis [9]. While this design seems to be quite robust, it comes in conflict with energetic restrictions posed by the existing theories of electron transfer in solutions [4].

The current paradigm in the field goes back to the classical work of Marcus [10], where the framework for understanding electron transfer between ions in solution was established. The main conceptual foundation of this theory is the idea that a non-equilibrium fluctuation of the medium needs to occur to bring the donor and acceptor electronic energy levels into resonance with each other. The free energy required for such a fluctuation is determined by two parameters: the reaction free energy (free energy difference between the products and reactants) and the free energy of reorganizing the medium, known as the electron-transfer reorganization energy. While the first parameter is well-defined, the reorganization energy requires closer attention. In fact, different ways to mechanistically define this parameter will occupy a significant portion of the forthcoming discussion.

The reorganization energy can be defined as the free energy (reversible work) required to reorganize the medium from the state at equilibrium with the electron on the donor to a non-equilibrium state in which the electron is still on the donor, but the nuclear coordinates of the medium are those which are achieved in equilibrium with the electron on the acceptor. We provide more discussion of this concept as well as alternative definitions below, but it suffices to note for this introductory discussion that the reaction free energy needs to be equal to the negative of the reorganization energy to achieve an activationless reaction. The main mechanistic problem of this requirement for the biological design is that the thermal bath (protein, water, bilipid membrane, etc.) influencing the electron localized at the cofactor is soft and highly deformable (polarizable). This softness, and the related ability to polarize, leads to a high value

of the reorganization energy, of the order of ~ 1 eV. Therefore, the requirement of a negative reaction free energy ~ -1 eV to achieve activationless electron transfer in a single step is inconsistent with a relatively low free energy input of $\sim 1.1 - 1.4$ eV for the entire chain. This energy input needs to be applied to a potentially large number of electron-transfer steps in the cross-membrane electron transport, with many of them requiring low activation barriers. There is a clear energetic bottleneck that needs to be resolved. The question posed by this energy mismatch is: How does biology produce energy?

The arguments presented above are based on the Marcus model which fully relies on equilibrium thermodynamics, i.e., on the ability to find the free energy penalty invested in creating a non-equilibrium configuration to allow electron tunneling. This framework requires all nuclear modes coupled to the reaction coordinate to sample the entire phase space consistent with the conservation laws and contribute to the free energy with the weight specified by the equilibrium Gibbs ensemble. This requirement is very restrictive to the design of the electron transport chain, and we argue below that natural systems have overcome this difficulty by operating at the conditions of ergodicity breaking (nonergodicity) when equilibration of the bath modes coupled to the reaction coordinate is incomplete. Bath nonergodicity eliminates the link between the averages and fluctuations stipulated by the fluctuation-dissipation theorem [11, 12, 13, 14]. The mechanistic consequence for electron transport is a less stringent demand for negative reaction free energies in individual electron-transfer steps.

The notion that biochemical reactions might operate at conditions of nonergodicity in respect to the surrounding thermal bath opens up several avenues of fundamental significance. First, nonergodicity makes the Gibbs ensemble inapplicable and new rules for performing statistical averages need to be formulated. Some of these difficulties have been recognized, and solutions to them proposed, in the theory of glass materials [14]. *Discontinuous* ergodicity breaking was introduced in the theory of glass transition. It corresponds to separating the system phase space into components [15], with the statistical weight of the Gibbs ensemble applied to each component separately. As the liquid cools down, some of these components become unreachable on the time-scale of the experiment. Similarly, different conformational states of a protein carry close resemblance to components of a glass-former, and a conceptual link between bulk glass-formers and proteins has been established in the past [16, 17].

In addition to the ability to separate the phase space into components locked from observation by a given relaxation experiment, proteins as thermal bath introduce an additional phenomenology of *continuous* ergodicity breaking. This issue becomes important in view of the dispersive dynamics of proteins [18, 19, 20], which implies the existence of many, often overlapping, relaxation processes. Mechanistically it entails that once the protein is trapped within a few components available to a given relaxation process, fine-tuning of the phase space within these components is further required based on the reaction rate if some parts of the components' phase space cannot be reached on the time of the reaction. This phenomenology requires a separate statistical formalism

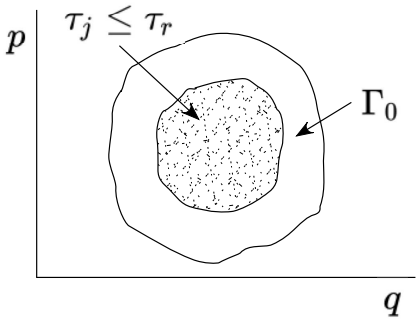

Figure 1: Schematic representation of the phase-space constraints required in the formalism of nonergodic activated kinetics. The phase space (q, p) in coordinates q and the momenta p available to the component is Γ_0. The reaction rate limits the phase space available for sampling by the requirements of the relaxation times τ_j to be shorter than the reaction time τ_r.

of *dynamically restricted ensembles* [21]. When applied to activated transitions, the dynamically restricted ensemble leads to *nonergodic activated kinetics* [21, 22]. The main consequence of this perspective is the dependence of the activation barrier on the reaction rate and the need to formulate a self-consistent scheme to calculate the rate.

Nonergodic kinetics, which extends the transition-state theory to activated transitions in dynamically dispersive media, brings the notion of the bath dynamics to the calculation of the reaction barrier. Dynamics is a recent newcomer to this field, in which the Gibbs energy has dominated the traditional thinking [23]. Given the importance of the bath dynamics in this new paradigm, one has to clarify what kind of dynamics is considered. The bath dynamics is understood here as defined by time correlation functions of the bath modes $q_j(t)$ coupled to the reaction coordinate. This view is distinct from the the mechanistic view of the dynamics in terms of the frequencies of normal modes of molecular vibrations Ω_j often adopted in molecular biophysics [24]. The distinction is easy to appreciate for an overdamped normal mode $q_j(t)$ described by the Langevin equation

$$\zeta_j \dot{q}_j + \Omega_j^2 q_j = y_j, \tag{1}$$

where y_j is a random force. The standard solution of this equation [25] produces the time correlation function $\langle \delta q_j(t) \delta q_j(0) \rangle \propto \exp[-t/\tau_j]$. Its exponential time decay is controlled by the relaxation time $\tau_j = \zeta_j / \Omega_j^2$, which depends on both the eigenfrequency Ω_j and the friction ζ_j. In contrast to the mechanical oscillatory dynamics of normal modes, dissipative dynamics require the rate of energy dissipation specified by friction. Relaxation processes in condensed media are often dominated by such overdamped modes with exponential (Debye) correlation functions [26, 27].

Once the relaxation times τ_j of the modes coupled to the reaction coordinate have been specified, one can proceed with defining the restricted phase space contributing to the statistical averages (figure 1). The reaction barrier is affected only by the processes that have their relaxation times τ_j shorter than the reaction time $\tau_r = k^{-1}$

required for the system to climb the activation barrier, which is given by the reaction constant k. Therefore, the dependence on the medium dynamics enters the activation barrier through a set of dimensionless parameters $k\tau_j$. The fast modes with $k\tau_j \ll 1$ contribute to driving the system over the barrier, while the slow modes with $k\tau_j \gg 1$ become dynamically frozen. They do not contribute to the barrier, but their effect potentially enters through the heterogeneous average of kinetic population traces over individual proteins. The statistical ensemble average used for the reaction barrier and the heterogeneous average over dynamically frozen coordinates affect the observables in different ways. These two types of statistical averages need to be considered separately.

The rates are expected to change significantly, and therefore can be controlled, near the points of dynamical resonances $k\tau_j \simeq 1$. Of course, the ability to control the rate by the medium dynamics is also determined by how large a change of the activation barrier can be achieved by dynamical freezing or unfreezing of a particular mode. It turns out that hydrated proteins are very special thermal media in this regard. They not only are characterized by a nearly continuous spectrum of dissipative relaxation times τ_j, but also produce strong electrostatic fluctuations at the active sites driven by the protein-water interface. It is this special nature of the protein-water interface that makes the dynamical control of chemical reactivity by natural enzymes particularly efficient.

Electrons are clearly not the only charged particles transferred across the membrane. The ultimate goal of photosynthesis and respiration is to produce the cross-membrane electrostatic potential and the gradient of proton concentration [3]. Protons are either consumed from the solution in proton-coupled redox reaction upon arrival of electrons or are actively pumped across the membrane. Protonation and deprotonation of residues and cofactors, altering their electrical charge when electrons are transferred, also helps in reducing the polarization stress of an extra molecular charge and can potentially make the reaction free energy more favorable to the overall efficiency. These mechanistic issues of proton-coupled electron transfer are important for a particular biochemical reaction mechanism [28], but are not considered here. We instead focus on the statistics, structure, and dynamics of the protein-water bath affecting active sites participating in electronic transitions. The general principles discussed here apply to any charged particles localized inside the protein and are extendable to reactions of proton transfer and proton-coupled electron transfer. Such extensions of the general ideas discussed here to these more complex reactions still await future studies. Here, we review the development of basic concepts over the last ten years since author's first publication on this subject [29].

2. General concepts of electron transfer

Electron transfer belongs to a broad class of processes in which the electron moves between localized states without absorbing a photon of electromagnetic radiation. This process is therefore a radiationless tunneling transition [30]. The electron tunnels between the donor and the acceptor when their energies are brought in resonance by

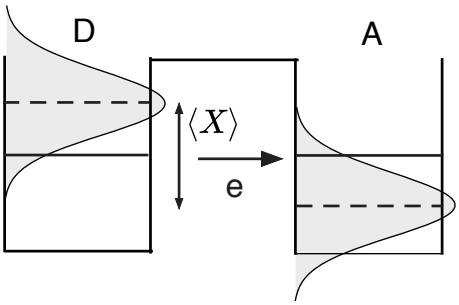

Figure 2: Diagram illustrating activated electron transfer in condensed media. The average energy gap $\langle X \rangle$ between the donor (D) and acceptor (A) sites of electron localization is no-zero. The resonance condition for electron tunneling, $X = 0$, is achieved due to thermal fluctuations of the bath nuclear coordinates coupled to the localized electron. These fluctuations create broadening of each electronic states indicated by shadowed areas. The probability of tunneling in the Gaussian picture is determined by two parameters: the average gap $\langle X \rangle$ and the gap variance σ_X^2 (equations 2 and 3).

thermal fluctuations (figure 2). The difference between these energies, known as the donor-acceptor energy gap X, becomes a natural choice for the reaction coordinate monitoring the progress of the reaction [31, 32]. The nuclear configuration at which electron tunneling becomes possible corresponds to zero energy gap, $X = 0$, which becomes the activated state of the electron-transfer reaction. The average energy gap $\langle X \rangle$ is generally non-zero and, therefore, a thermal fluctuation of the bath is required to bring the system to the state of $X = 0$.

According to the Onsager principle of microscopic reversibility, the average regression of spontaneous fluctuations obeys the same laws as the corresponding irreversible process [11]. One therefore can envision the rise and decay of spontaneous fluctuations as an equivalent process produced by an external force driving the system to a nonequilibrium configuration [10]. The probability of a spontaneous fluctuation is directly related to the reversible work required to produce the equivalent nonequilibrium configuration by applying an external force. In application to electron transfer, the probability $P(X) \propto \exp[-\beta F(X)]$ of a fluctuation resulting in the donor-acceptor energy gap X is determined by the free energy, or reversible work, $F(X)$ required to produce the same configuration by applying an external force ($\beta = 1/(k_{\rm B}T)$, $k_{\rm B}$ is Boltzmann's constant and T is the absolute temperature).

If the electronic states of the donor and acceptor are coupled to a sufficient number of particles in the bath, the statistics of the stochastic variable X should approach the Gaussian limit (central limit theorem) with the mean $\langle X \rangle$ and the variance σ_X^2

$$P(X) \propto \exp\left[-\frac{(X - \langle X \rangle)^2}{2\sigma_X^2}\right]. \tag{2}$$

The activation barrier for the tunneling transition is then obviously given by the ratio

of probabilities to obtain the zero and average energy gap

$$\beta F^{\rm act} = -\ln\left[P(0)/P(\langle X\rangle)\right] = \frac{\langle X\rangle^2}{2\sigma_X^2}. \tag{3}$$

The probability of the resonance can be combined with the probability of tunneling when the resonance is reached within the Golden Rule perturbation scheme of quantum mechanics, with the result for the rate of (nonadiabatic [5]) electron transfer

$$k \propto V^2 e^{-\beta F^{\rm act}}. \tag{4}$$

Here, V is the electron-transfer matrix element (donor-acceptor electronic coupling) connected to the probability of tunneling and exponentially decaying [5, 33, 34] with the donor-acceptor distance R: $V \propto \exp[-\gamma R]$. The design of natural electron transport chains is ultimately driven by balancing the needs of maximizing V and minimizing $F^{\rm act}$ [35].

The arguments presented so far are quite general and are limited only by the assumption of the Gaussian statistics of the stochastic variable X. The next step commonly performed in formulating the theory is to assume that the Gibbs ensemble can be used to calculate the mean and the variance of X in (2). We will show below that the use of the standard Gibbs ensemble is often not justified for electron transfer driven by nuclear fluctuations of the protein-water stochastic ensemble. A more subtle formulation, taking into account the separation of the relevant time-scales and formalized in terms of the dynamically restricted statistical ensemble, is discussed below. We first start with outlining the consequences of using the conventional Gibbs ensemble for statistical averages in electron transfer rates.

If the Gibbs ensemble is used to calculate averages over the nuclear configurations of the system, the Hamiltonian of the system determines the statistical weight $\rho_i \propto \exp[-\beta H_i]$ of a given configuration. Here, we distinguish between the initial state when the electron is on the donor, H_1, and the final state when the electron is on the acceptor, H_2. The energy gap $\Delta H(\Gamma) = H_2(\Gamma) - H_1(\Gamma)$ depends on the instantaneous nuclear configuration of the system determined by all phase-space coordinates lumped into Γ. The progression of the reaction can be gauged by how close the system has approached the tunneling configuration of $X = 0$.

Using the Gibbs ensemble to weigh the statistical configurations, the probability distribution in (2) can be calculated by summing up all possible nuclear configurations Γ constrained to produce a given value of the energy gap $X = \Delta H(\Gamma)$. This is mathematically achieved by using the delta-function in the statistical integration as follows

$$P_i(X) = e^{-\beta F_i(X)} \propto \int \delta\left(\Delta H(\Gamma) - X\right) \rho_i(\Gamma) d\Gamma. \tag{5}$$

An important relation between two probabilities [36], discussed by Warshel and Tachiya [32, 37], follows from this definition. The free energies $F_i(X)$ satisfy the "energy conservation" relation

$$F_2(X) = F_1(X) + X. \tag{6}$$

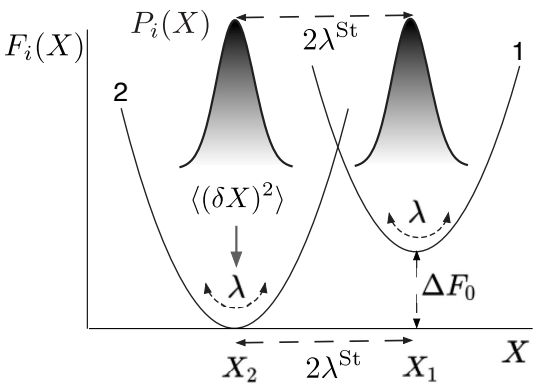

Figure 3: Diagram of the free energy surfaces of electron transfer $F_i(X)$. The distance between parabola's minima is the "Stokes shift" reorganization energy λ^{St}. The curvature of the parabolas is related to the reorganization energy $2\lambda = \left[\partial^2 F_i(X)/\partial X^2\right]^{-1}$. In optical spectroscopy, $2\lambda^{\mathrm{St}}$ is the Stokes shift between the peaks of optical lines represented by the probability functions $P_i(X = \hbar\omega)$. The vertical displacement between the parabolas' minima yields the reaction free energy $\Delta F_0 = F_{02} - F_{01}$.

Apart from the formal derivation directly following from (5), this equation expresses the fact that the "vertical" transition at fixed nuclear coordinates (and fixed X) should not change the entropy of the system. Therefore $\Delta F = F_2 - F_1 = X - T\Delta S = X$, or $\Delta S = 0$. The gap between two free energy surfaces at fixed nuclear coordinates does not involve an entropy component and is identically equal to the amount of energy supplied to the system to move the electron to an energy state different from its current state. This statement implies energy conservation, which is the physical meaning of (6).

The combination of the energy conservation condition (6) with the assumption of the Gaussian character of the variable X leads to particularly simple forms of the free energy surfaces $F_i(X)$. Before producing these equations, we start with an additional simplification of the algebra by applying the Nyquist theorem [11, 13] stating that the noise of a classical stochastic variable should be proportional to temperature. More specifically, the variance σ_X^2 is expected to carry linear dependence on temperature

$$\sigma_X^2 = 2k_{\mathrm{B}}T\lambda. \tag{7}$$

The energy parameter λ, quantifying the magnitude of the energy gap fluctuations, is the electron-transfer reorganization energy. The combination of the Gaussian statistics of X with the Nyquist theorem brings the free energy surfaces $F_i(X)$ to the form originally suggested by Marcus [10]

$$F_i(X) = F_{0i} + \frac{\delta X^2}{4\lambda}, \tag{8}$$

where $\delta X = X - \langle X\rangle_i$ and F_{0i} define the vertical positions of two parabolas, i.e., the free energies at the minima. The reorganization energy λ in the denominator determines the curvatures of the parabolas (figure 3).

If (6) is next applied to two free energy surfaces in (8), one gets two additional

constraints on the values of the average energy gaps $\langle X\rangle_i$ and the free energies F_{0i}

$$2\lambda^{\mathrm{St}} = \langle X\rangle_1 - \langle X\rangle_2 = 2\lambda \tag{9}$$

and

$$\Delta F_0 = F_{02} - F_{01} = \tfrac{1}{2}\left(\langle X\rangle_2 + \langle X\rangle_1\right). \tag{10}$$

The first relation gives the horizontal displacement between the minima of the two parabolas. By the choice of the reaction coordinate, this distance is also the difference in the vertical transition energies, i.e., the Stokes shift between emission and absorption maxima reported by optical spectroscopy [38]. Therefore, we use the subscript "St" to label this energy, which we call the "Stokes shift reorganization energy". It is thus based on the first moments of the vertical transition energy in contrast to λ in equations (7) and (8) based on the variance of X, i.e., on the second moment. The variance is spectroscopically reported by the inhomogeneous width of spectral lines. Therefore, λ^{St} and λ can be separately extracted from the analysis of band-shapes of charge-transfer optical lines [39].

Equation (8) can also be used to obtain the original Marcus definition of the reorganization energy [4, 10]. As we mentioned above, it is given by the free energy invested to move the system along its initial-state free energy surface to the nuclear configuration of the final state. In other words, one has to put $\delta X = \langle X\rangle_1 - \langle X\rangle_2 = 2\lambda^{\mathrm{St}}$ in (8). The result is

$$\lambda^{\mathrm{M}} = \frac{(\lambda^{\mathrm{St}})^2}{\lambda}. \tag{11}$$

Equation (9) constrains the curvatures of the parabolas and their horizontal displacement to be determined by a single parameter $\lambda^{\mathrm{St}} = \lambda$ also equal to the Marcus reorganization energy in (11). In addition, equation (10) connects the coordinates of parabolas' minima $\langle X\rangle_i$ with their vertical displacement, i.e., the reaction free energy ΔF_0 (figure 3). The theory of electron transfer in this formulation requires any two independent parameters out of four parameters $\langle X\rangle_i$, λ, ΔF_0 describing the Gaussian statistics of the energy gap. For instance, the activation barrier of the forward $(1 \to 2)$ reaction is given in terms of two independent parameters λ and ΔF_0

$$F^{\mathrm{act}} = \frac{(\lambda + \Delta F_0)^2}{4\lambda}. \tag{12}$$

Here and below we drop the state index $i = 1$ in the activation energy for brevity.

Equation (9) is the static ($t \to \infty$) limit of the fluctuation-dissipation theorem [11, 13, 14]. It links the time-dependent linear response of an observable to a small external perturbation through the time correlation function of the unperturbed system. In this framework, λ^{St} represents the linear response (first moment), while λ quantifies the amplitude of the fluctuations (second moment). It has been established that separating the phase space of the systems into non-overlapping subsets, known as components [14, 15], invalidates the fluctuation-dissipation relation [14]. Making parts of the phase space inaccessible amounts to ergodicity breaking, which renders the Gibbs

ensemble inapplicable for the calculation of statistical averages. One of the consequences of this new physics is that one has to consider $\lambda^{\rm St}$ and λ as separate parameters, often widely different in magnitude. As we discuss below, the separation of $\lambda^{\rm St}$ and λ allows electron transport to proceed with significantly lower losses of the free energy between the points of input and output. Once the grip of thermodynamics and equilibrium ensembles on the description of electron transport is released, significant improvements in the energetic efficiency of electron transport become possible. On a more fundamental level, this conceptual framework also opens the door to control enzymetic reactions by the bath dynamics.

3. Gibbs ensemble, broken ergodicity, and Gaussian fluctuations

The separation of the reaction coordinate from a manifold of all possible degrees of freedom of the system in (5) requires a certain separation of time scales. Integrating out a subset of coordinates under the constraint $\Delta H(\Gamma) = X$ assumes that one can keep X fixed while performing the statistical average. This assumption implies that all those bath coordinates relax faster than the reaction evolving along the reaction coordinate X. When these restrictions do not hold, ergodicity breaks down, as has been recognized in the past [14, 15]. For instance, in the case of a phase transition, a part of the phase space that becomes forbidden by symmetry breaking is kinetically inaccessible (essentially infinite time is required to flip the dipoles of a macroscopic ferromagnet). A biasing field, artificially breaking the symmetry, needs to be added to the Hamiltonian to drive the system to the correct part of the phase space. Another example is the glass transition, when a part of the phase space becomes kinetically inaccessible on the observation time-scale [16]. In order to accommodate these difficulties, constraints to the statistical ensemble are introduced by splitting the phase space into components such that equilibrium sampling is allowed in each of them [15]. The free energy can then be defined for a given component Γ_0 by restricting the phase space integration (figure 1)

$$e^{-\beta F(\Gamma_0)} = \int_{\Gamma_0} e^{-\beta H(\Gamma)} d\Gamma. \tag{13}$$

The ensemble restricted to Γ_0 is then a nonequilibrium ensemble. The system evolves to the equilibrium ensemble by aging dynamics, which samples different components in the phase space through activated transitions between them.

The general phenomenon of glass transition and related glassy dynamics [16] are most relevant to the difficulties encountered when formulating activated kinetics in a dynamically dispersive thermal bath. However, the problem here is potentially more complex than ergodicity breaking in both phase and glass transitions. In the former case, ergodicity breaking is pre-defined by the symmetry, in the latter case the separation into components can be specified. Both cases represent discontinuous ergodicity breaking, i.e., the condition when the separation of the phase space into parts is well-defined. In contrast, ergodicity breaking in highly dispersive media can be

continuous, i.e., the part of the phase space where Gibbs ensemble sampling is allowed can be continuously adjusted as the rate of the process changes. Since the activation barrier is affected by the phase space sampled by the system, the nonergodic kinetics introduced below self-consistently adjusts the rate to the part of the phase space where the Gibbs ensemble is allowed [21]. This self-consistent procedure is made possible by introducing a dynamically restricted ensemble with the constraint on the phase space established through the rate.

The standard definition of the phase space in classical statistical mechanics is a collection of all coordinates $q_i(t)$ and their corresponding conjugated momenta $p_i(t)$ evolving in time according to the equations of motion. A mathematically equivalent representation is in terms of corresponding time Fourier transforms $q_i(\omega)$ and $p_i(\omega)$. Statistical average in this latter representation requires integrating over all coordinates and momenta for all frequencies of the Fourier transform space

$$d\Gamma = \prod_{\omega} \prod_{i} dq_i(\omega) dp_i(\omega). \tag{14}$$

This representation immediately suggests an extension to a dynamically restricted ensemble [21]. The new definition of the statistical average is achieved by restricting the range of frequencies in the integral to the frequencies above the reaction rate k

$$d\Gamma_k = \prod_{\omega>k} \prod_{i} dq_i(\omega) dp_i(\omega). \tag{15}$$

Correspondingly, the dynamically restricted statistical average becomes

$$\langle \dots \rangle_k = Z_k^{-1} \int \dots e^{-\beta H(\Gamma)} \prod_{\omega>k} \prod_{i} dq_i(\omega) dp_i(\omega), \tag{16}$$

where $Z_k = \int \exp[-\beta H(\Gamma)] d\Gamma_k$.

The formulation of statistical averages according to equations (15) and (16) permits continuous ergodicity breaking by diminishing the number of configurations accessible to the system on the time of observation, which is the time of the reaction $\tau_{\rm r} = k^{-1}$ for a chemical transformation with the reaction rate k. Since the rate constant depends on statistical averages through the activation barrier, it needs to be calculated from a separate self-consistent formalism of nonergodic activated kinetics discussed below. The bath dynamics enter the calculations through the set of relaxation times of the bath τ_j. The slow modes with $k\tau_j \gg 1$ do not contribute to the statistical average and remain frozen on the time-scale $\tau_{\rm r}$. The actual values of these dynamically frozen coordinates will depend on the initial preparation of the system. For instance, the slow coordinates belong to the Gibbs distribution in equilibrium with the donor's ground state when fast electron transfer is promoted by absorption of light in bacterial photosynthesis.

In order to illustrate how actual calculations are performed, we start with the loss spectrum $\chi''_X(\omega)$ (figure 4) of the energy gap fluctuations in the bacterial reaction center [40]. The loss function is calculated from the time autocorrelation function

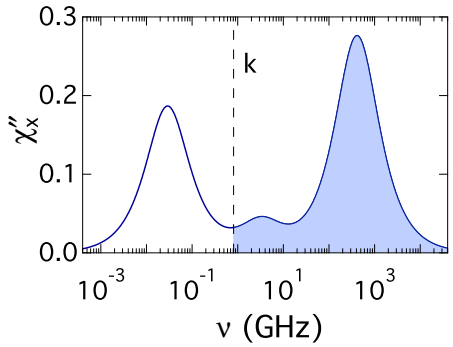

Figure 4: Loss spectrum of the energy-gap dynamics of the charge shift reaction between the reduced bacteriopheophytin (H_A^-) and the active-side quinone (Q_A) cofactors (see figure 17). The reaction is studied by MD simulations of the wild-type reaction center of *Rhodobacter sphaeroides* [40]. The loss function $\chi''_X(\nu)$ is plotted vs $\nu = \omega/(2\pi)$. The vertical dashed lines indicate the value of the experimental rate constants $k/(2\pi)$ and the shaded area marks the frequencies contributing to the statistical average defined on the dynamically-restricted ensemble.

$C_X(t) \propto \langle \delta X(t)\delta X(0)\rangle$ by taking the Fourier transform $\tilde{C}_X(\omega)$: $\chi''_X(\omega) \propto \omega\tilde{C}_X(\omega)$. Each peak ω_j in the loss spectrum corresponds to a Debye relaxation process with the relaxation time $\tau_j = \omega_j^{-1}$ from a multi-exponential fit of $C_X(t)$. Some of these processes are faster than the observable reaction rate, $\omega_j > k$, but some are slower than the rate, $\omega_j < k$. The slower processes are eliminated from the statistical average and the corresponding fluctuations do not contribute to the energy gap variance. One therefore needs to introduce the nonergodic reorganization energy $\lambda(k)$ [29, 21]

$$\lambda(k) = \int_k^\infty \chi''_X(\omega)(d\omega/\pi\omega). \tag{17}$$

It is clear from figure 4 that $\lambda(k) < \lambda$ at $k > 0$. One recovers the thermodynamic value of the reorganization energy, $\lambda(k) \to \lambda = \lambda(0)$, in the limit of an infinitely slow reaction, $k \to 0$, corresponding to the Gibbs ensemble.

The dynamics of proteins are often heterogeneous, as manifested by stretched correlation and loss functions [20] and fractal dimensions of vibrational densities of states [19]. Such complex loss functions affect the reaction activation through the integral in (17), which is not very sensitive to the details of the relaxation dynamics. The use of stretched functions from the measured liquid relaxation to predict spectroscopic line-shapes in the spirit of equation (17) provides good account of observations [41]. In the less challenging case of multi-exponential Debye relaxation, $C_X(t)$: $C_X(t)/C_X(0) = \sum_j A_j \exp[-t/\tau_j]$, equation (17) can be converted to a convenient analytical form

$$\lambda(k) = \lambda \sum_j (2A_j/\pi)\mathrm{arccot}(k\tau_j), \tag{18}$$

where $\sum_j A_j = 1$. It is easy to see that slow relaxation processes with $k\tau_j \gg 1$ do not contribute to $\lambda(k)$.

It is clear from the discussion that the thermodynamic free energy is not involved in the formation of the barrier when ergodicity is broken and only fast nuclear modes sample the phase space. The reliance of biochemitry and chemical kinetics on thermodynamics to describe the reaction free energy and heat is of limited use in such cases [40]. Instead, the reaction free energy $\Delta F(k)$ ($\Delta F(0) = \Delta F_0$) gains the dependence on the reaction rate. In application to electron transfer, this requirement follows from the observation, discussed above, that $\lambda(k)+\Delta F(k)$ should give the average *energy* gap, i.e., the entropy components have to mutually cancel out.

It is instructive to illustrate equation (17) with the example of a harmonic oscillator. The free energy invested in displacing a harmonic oscillator by the extension Δq is $\beta\Delta F = (\Delta q)^2/2\langle\delta q^2\rangle$. This equation carries the same structure as (2) and (3), which are valid for a general Gaussian stochastic variable. The variance $\langle\delta q^2\rangle$ can be written as the frequency integral of the frequency Fourier transform $\tilde{C}_q(\omega)$ of the time autocorrelation function $C_q(t) = \langle\delta q(t)\delta q(0)\rangle$: $\langle\delta q^2\rangle = \int_0^\infty \tilde{C}_q(\omega)(d\omega/\pi)$. The loss function is defined from the correlation function as $2\chi_q''(\omega)/\omega = \beta\tilde{C}_q(\omega)$ [12]. Therefore, one gets for the variance

$$\langle\delta q^2\rangle = 2k_{\rm B}T\int_0^\infty \chi_q''(\omega)(d\omega/\pi\omega). \tag{19}$$

A lower frequency cut-off needs to be introduced into this integral when the observation window is finite, as in (17). This procedure accounts for the specific instrumental observation window and is a special case of a general phenomenon of nonergodicity. It was successfully applied to the temperature alteration of the harmonic displacement of the iron atom in heme proteins measured by Mössbauer spectroscopy [17, 42]. The phenomenology here is exactly the same as for the nonergodic reorganization energy in (17), except that the frequency range is fixed by the instrument and is not continuously adjusted. The relaxation time falls out of the instrumental window with lowering temperature, resulting in the dynamical freezing of the corresponding nuclear modes and a drop in the magnitude of the atomic displacement. This phenomenon is generally known as dynamical transition in proteins and is also observed in displacements of protein hydrogen atoms recorded by neutron scattering [43].

Continuous ergodicity breaking is not the only possible but a conceptually more challenging scenario than the more common discontinuous ergodicity breaking [15]. As discussed above, the latter is realized when the configuration space can be divided into well-defined components separated by barriers. It requires a complex topology of the configuration space characterized by several reaction coordinates with widely different relaxation times. The basins in the configuration space that are separated by high barriers are not visited on the reaction time-scale and must be excluded from the statistical average (figure 5).

This situation is important for proteins, where the two major sets of coordinates can be related to the medium polarization and conformational transitions. These two types of collective nuclear modes are characterized by widely different relaxation times, from picoseconds to nanoseconds (or even microseconds [44]) for the polarization response

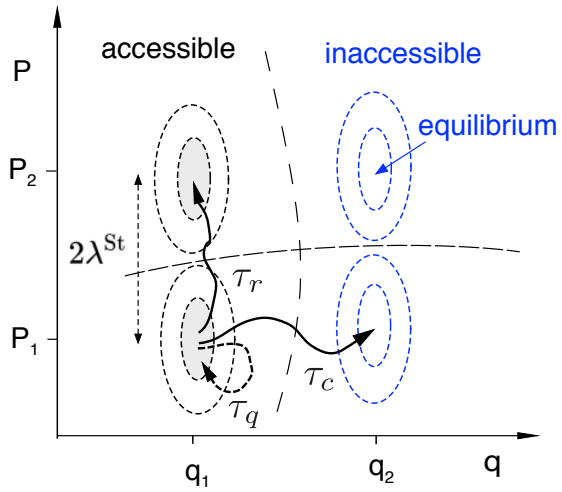

Figure 5: Schematic representation of ergodicity breaking for electron transfer in the space of two reaction coordinates: the fast coordinate of the interfacial polarization P and the slow coordinate of the conformational transitions q. The dashed lines indicate the barriers between the basins corresponding to local minima in the $q-P$ space. The points (q_1, P_1) and (q_2, P_2) denote two different electron-transfer states fully equilibrated with P and q nuclear coordinates. The second, (q_2, P_2), state is not accessible on the reaction time-scale τ_r and the state (q_1, P_2) is reached instead. The separation of the minima determines the Stokes shift, $2\lambda^{\rm St}$. The ergodicity is broken because $\tau_c \gg \tau_r$ (discontinuous ergodicity breaking). However, $\tau_r > \tau_q$ and elastic fluctuations with the relaxation time τ_q affect the donor acceptor energy gap resulting in $\kappa_G = \lambda/\lambda^{\rm St} \gg 1$. In cases when τ_r is lower then some subset of relaxation times τ_{pi} (P-coordinate) and τ_{qi} (q-coordinate), continuous ergodicity breaking occurs, affecting the rate of transition along the reaction coordinate P. The constrains on the available configuration space in that case are schematically shown by the shaded area.

vs milliseconds for conformational changes. Further, the times of fluctuations near the equilibrium and the times of reaching the minima separated by high barriers can be widely different [45]. One can therefore consider a situation when fluctuations along the slow reaction coordinate, which can potentially populate the barrier-separated minima, are realized on the observation time, but the transitions overcoming the barriers are not.

Figure 5 illustrates this situation in terms of two reaction coordinates, a fast polarization coordinate P and a slow conformational coordinate q. The configuration space is separated into basins corresponding to equilibria along P and q in respect to two localizations of the electron, either on the donor (reactant state, $i = 1$) or on the acceptor (product state, $i = 2$). The basins are separated by the corresponding activation barriers, but the barriers separating the basins along the conformational coordinate are much higher than the barriers separating different polarization states. Clearly, reaching a new conformation requires a much longer time τ_c, often measured in milliseconds [46], compared to the reaction time τ_r required to change the redox state along the reaction coordinate P. At the same time, the relaxation time along the conformational reaction coordinate τ_q can still be lower than the reaction rate τ_r:

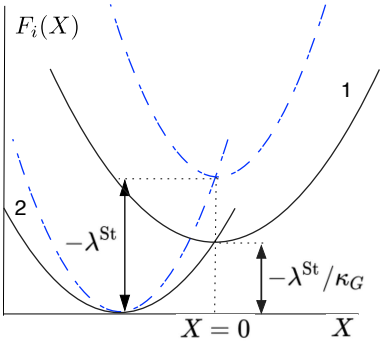

Figure 6: Free energy surfaces of activationless electron transfer with $\kappa_G > 1$ (solid lines) compared to the Marcus result of $\kappa_G = 1$ (dash-dotted lines); $\kappa_G = \lambda/\lambda^{\mathrm{St}}$.

$\tau_q \ll \tau_{\mathrm{r}} \ll \tau_{\mathrm{c}}$. This is the scenario in which fluctuations along the coordinate q are accessible on the reaction time-scale, but the conformational minima are not.

Under this particular separation of time-scales the fluctuations of the interfacial polarization P are modulated by conformational fluctuations along the coordinate q. This modulation is particularly efficient in the case of the protein water-interface, where protein's elasticity is coupled with the polarization of water by the charged surface residues. We discuss the specifics of this coupling below, but the main mechanistic consequence of this specific form of discontinuous ergodicity breaking is the separation between two reorganization energies λ^{St} and λ, leading to the following inequality

$$\kappa_G = \lambda/\lambda^{\mathrm{St}} > 1. \tag{20}$$

It is this phenomenology that allows proteins to avoid losing the free energy in electron-transfer transitions and to improve the overall energetic efficiency of electron transport [47].

The mechanistic consequence of inequality (20) is illustrated in figure 6. The free energy surfaces are much broader than prescribed by assuming $\lambda^{\mathrm{St}} = \lambda$. If the surfaces are still parabolic, as suggested by MD simulations [47], the only constraint on the free energy surfaces that remains is the requirement to cross at $X = 0$: $F_1(0) = F_2(0)$ in equation (8). From this requirement, one gets the relations connecting the average values of the energy gap to the reorganization energies and the reaction free energy

$$\begin{aligned} \langle X\rangle_1 &= \kappa_G \Delta F_0 + \lambda^{\mathrm{St}}, \\ \langle X\rangle_2 &= \kappa_G \Delta F_0 - \lambda^{\mathrm{St}}. \end{aligned} \tag{21}$$

Correspondingly, the activation barrier of the forward ($1 \to 2$) reaction changes from equation (12) to the following relation

$$F^{\mathrm{act}} = \frac{\langle X\rangle_1^2}{4\lambda} = \frac{(\lambda^{\mathrm{St}} + (\lambda/\lambda^{\mathrm{St}})\Delta F_0)^2}{4\lambda}. \tag{22}$$

Instead of two parameters, $\lambda = \lambda^{\mathrm{St}}$ and ΔF_0, required to determine the activation free energy in the standard Marcus model [4], the new equation involves three parameters,

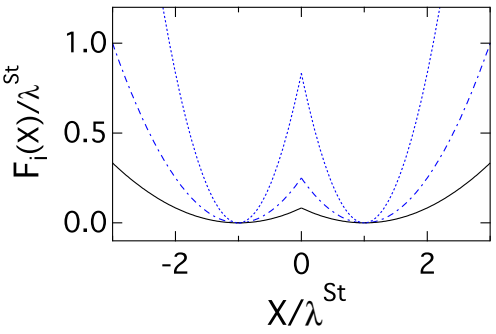

Figure 7: Free energy surfaces of self-exchange electron transfer ($\Delta F_0 = 0$) with $\kappa_G > 1$ (solid lines) compared to the Marcus result of $\kappa_G = 1$ (dash-dotted lines, $F^{\rm act}/\lambda^{\rm St} = 1/4$) and to $\kappa_G < 1$ (dotted line); $\kappa_G = \lambda/\lambda^{\rm St}$. The activation barrier continuously drops with increasing κ_G (equation (23)).

with two distinct reorganization energies. The activation barrier of the backward reaction $F_2^{\rm act}$ is obtained by replacing $\langle X\rangle_1$ with $\langle X\rangle_2$ in (22). The detailed balance is obviously maintained, $F_1^{\rm act} - F_2^{\rm act} = \Delta F_0$. Other mechanistic consequences of the three-parameter model can be illustrated by two special cases.

In the case of self-exchange electron transfer, characterized by zero reaction free energy $\Delta F_0 = 0$, one gets

$$F^{\rm act} = \frac{\lambda}{4(\kappa_G)^2} = \frac{\lambda^{\rm St}}{4\kappa_G}. \tag{23}$$

The activation barrier in this case is lowered by $\kappa_G > 1$ compared to the standard result of the Marcus theory [4], $F^{\rm act} = \lambda^{\rm St}/4$ (equation (12)). This is illustrated in figure 7. The values of $\lambda^{\rm St}$ in the range $\lambda^{\rm St} \sim 0.7 - 1.0$ eV are typically found for proteins. The corresponding reorganization energies λ are significantly higher [47, 48], with κ_G varying between proteins [42], but can be as high as $\kappa_G \simeq 5$ (see also table 1 below). While most reactions are probably optimized toward $\kappa_G > 1$ to allow faster electron flow, one can anticipate situations when this is not desirable and electron needs to be localized on its carrier to avoid unwanted oxidation of the components of the cell. This can be achieved when $\kappa_G < 1$, which makes the barrier higher compared to the standard prediction (figure 7). Overall, more flexibility is provided by κ_G in (23) compared to the standard picture.

The second example is activationless electron transfer, $F^{\rm act} = 0$. Achieving this condition requires negative reaction free energy, $\Delta F_0 = -\lambda^{\rm St}$, according to the standard formulation (equation (12) and figure 6). As mentioned above, this requirement puts stringent constraints on the molecular design of the electron transport chain, which are resolved by allowing two separate reorganization energies. From equation (21), the free energy released in an activationless reaction, $\langle X\rangle_1 = 0$, becomes

$$\Delta F_0 = -\frac{\lambda}{\kappa_G^2} = -\frac{\lambda^{\rm St}}{\kappa_G}. \tag{24}$$

It is clear that $\kappa_G > 1$ lowers the amount of free energy lost in an electron-transfer step compared to $-\lambda^{\mathrm{St}}$ required by equation (12) (figure 6). More electron-transfer steps can be accomplished within a given free energy window and the energetic efficiency of the electron transport chain, i.e., the ability to keep electrons in high free energy states, is improved.

4. Nonergodic activated kinetics

Conceptual connection between proteins and fragile glass-formers has been emphasized in the past [49, 17, 50]. The similarity between these two functionally and structurally different systems is the presence of a "rugged landscape" [51], i.e., a high density of local minima on the surface of system's energy as a function of its coordinates (energy landscape) [45]. Thermal fluctuations of the bulk material can be viewed as an activated walk on this energy landscape, which occurs by continuous crossing of low and high barriers. The spread of the activation barriers leads to a large number of relaxation times and complex dynamics. Both features are commonly lumped into the notion of dispersive dynamics of the system. The question related to proteins is whether the microstates belonging to the same macrostate (folded structure) contribute only to the entropic part of the reaction free energy barrier [52, 53] or the random walk between the minima can potentially affect the observed reaction rate [54, 55].

This question does not have a simple resolution within the established framework of activated chemical kinetics [56]. The standard formulation of the transition-state theory prescribes that most of the medium's effect on the reaction rate is static and contributes to the free energy barrier, a thermodynamic property. Modifications of the transition-state theory, such as Kramers' diffusional dynamics [57], introduce dissipation and characteristic relaxation times into the preexponential factor of the rate, but do not affect the Arrhenius activation term, which remains the Boltzmann occupation probability of the transition state.

This general framework is shared by theories seeking to include solvent relaxation into the rate of electron transfer [58, 59, 60, 61, 62]. The relaxation of the medium polarization competes in these theories with the rate of electron tunneling [58], or with both the rate of tunneling and the frequencies of molecular skeletal vibrations of the donor and acceptor [59, 62]. The bath dynamics enters the rate preexponent and no significant control of the reaction rate by the protein dynamics is predicted by these theories. This perspective, generally consistent with the Kramers' theory, is the conceptual basis for the criticism of the proposition that protein dynamics may be a significant factor affecting the rate [52, 53, 63].

What is not fully appreciated by the standard models is that defining the free energy profile along a small set of reaction coordinates requires certain separation of time-scales and, in fact, breaking of ergodicity [15]. The situation here is completely analogous to the Landau theory of phase transitions [64]. Defining the free energy as a function of a set of order parameters (reaction coordinates) requires freezing them at

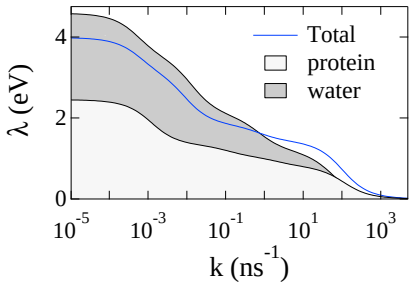

Figure 8: Nonergodic reorganization energy of electron transfer depending on the observation window allowed by the reaction rate constant k (equations (17) and (18)). The protein and water components of the reorganization energy are shown separately. The results are obtained from 13 μs atomistic MD simulations of the membrane-bound bc_1 complex of *Rhodobacter sphaeroides* bacterium [44].

certain values when the statistical averages are performed. Equations of motions using these free energies as potential surfaces also assume that the bath adjusts adiabatically to any change in the order parameters, i.e., a separation of the relevant time-scales is required.

The concept of free energy functionals defined by Gibbs ensembles with a subset of frozen reaction coordinates becomes unreliable when the reaction time falls in a dense spectrum of relaxation times. One has to face the problem of continuous ergodicity breaking [22, 21]: only the modes with the characteristic frequencies ω higher than the reaction rate contribute to the Gibbs ensemble. The free energy of activation is replaced with the activation energy $E_a(k)$, which depends on the rate constant k and the bath dynamics through the constraint imposed on the phase space by the condition $k < \omega$. How much $E_a(k)$ changes with the rate depends on the number of bath modes coupled to the reaction coordinate, on the coupling strength, and on the position of k within the spectrum of relaxation times τ_j (figure 4). It is at this point when the unique nature of hydrated proteins as thermal reservoirs comes into the picture.

A large number of often overlapping relaxation processes ensures a continuous and significant change of the barrier when the rate is tuned to optimize biological function. This is expressed mathematically by replacing the transition-state reaction rate by a self-consistent equation solved iteratively in respect to the unknown rate k [47, 65]

$$k = \omega_n \exp\left[-\beta E_a(k)\right]. \tag{25}$$

Here, ω_n is the characteristic frequency along the reaction coordinate at the reactant potential well [57]. For nonadiabatic electron transfer, the rate of reactants-to-products flux at the top of the activation barrier is dominated by the tunneling rate. The preexponential factor $\omega_n \propto V^2$ in this case is determined by the electron-transfer overlap V (equation 4). This limit is most relevant for protein electron transfer [33, 66]. The protein dynamics can affect the reaction rate both through modulating V [66] and through $E_a(k)$, but the latter effect is more significant.

For the dynamical control to be efficient, $E_a(k)$ needs to be a sufficiently steep function of k near the solution to the self-consistent equation (25). The ability of the protein-water thermal bath to provide such steep functions is illustrated by $\lambda(k)$ (equations (17) and (18)) shown in figure 8. This nonergodic reorganization energy was calculated from 13 μs simulations [44] of the rate-limiting electron transfer reaction in the membrane-bound bc_1 complex of *Rhodobacter sphaeroides* bacterium. The overall system is highly heterogeneous, with protein, water, lipids of the membrane, and ions in the solution all contributing to the fluctuations of the donor-acceptor energy gap on their corresponding time-scales. The dynamically dispersive spectrum of this thermal bath leads to an almost continuous change of the reorganization energy when longer observation times open up with decreasing reaction rate. Remarkably, half of the reorganization energy calculated from 13 μs of simulations comes from two slowest processes of the bath, with the relaxation times of 0.1 and 1.6 μs. It is quite possible that even slower relaxation processes, currently unreachable by computer simulations, contribute to the activation barrier. A significant contribution of slow modes to $\lambda(k)$ creates the potential for controlling relatively slow reactions by increasing the fraction of slow elastic modes in the protein's density of states, as we discuss in more detail below.

5. Structure and dynamics of the protein-water interface

The reorganization energy $\lambda(k)$ is a measure of the breadth of electrostatic fluctuations of the thermal bath observable on the reaction time $\tau_r = k^{-1}$. Its steep slope, which allows an efficient dynamical control of the activation barrier, originates from unique properties of the protein-water interface. Those, in turn, are a direct consequence of the requirement for these large molecules to be soluble in water. This is achieved by placing, in the process of protein folding, a high density of ionized (protonated and deprotonated) residues to the protein surface. The free energy of solvation of the surface charges provides the required free energy of protein solvation. The charged residues not only stabilize the protein in solution, but also significantly influence its hydration shell [67]. A typical globular protein carries $\simeq 500$ water molecules in its first hydration layer. This large number of molecules provides a large number of microscopic configurations. One can think of the protein hydration shell as a separate sub-ensemble of "biological water" [68] with properties significantly different from the bulk. Biological justification for this assignment comes from the observation of a highly crowded nature of some parts of the cell, such as the cytogel. The latter is a submembrane region with a high volume fraction of protein (40–90% [69]) comparable to that in a protein crystal [70]. Water in these regions of the cell can only exist as hydration (interfacial) water, which is corroborated by the name "biological water".

The protein-water interface that is the focus of our discussion here is an extended region incorporating $\sim$ 1 nm thick layer of perturbed "biological" water, but also including the surface layer of the protein. The interfacial perturbation of the protein structure related to hydration of side chains and ionized residues propagates fairly

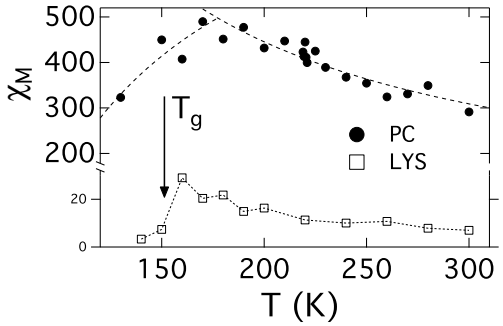

Figure 9: Dipolar susceptibility of the first hydration later of plastocyanin (PC) [73] and lysozyme (LYS) [74] vs temperature. The dotted lines are drawn to help the eye. Adapted with permission from [74]. Copyright 2015 American Chemical Society.

deep into the protein interior. The interior groups get more mobile with increasing hydration [71], and larger volumes become available for a single-well diffusion of the interior atoms [72]. The enhanced vibrational softness of the surface layer implies more intense fluctuations. Combined with the high density of charge from the protein residues and polarized water in this region, the interface becomes the main source of electrostatic noise affecting reaction sites inside the protein. The interface, as we understand it here, extends itself in two opposite directions from the dividing protein-water surface: into bulk water and into the protein interior.

The water density is higher in the hydration layer than in the bulk due to strong protein-water interactions and packing preferences [75]. These interactions also break the bulk-like network of hydrogen bonds, collapsing water's open structure in the hydration layer [76]. The breaking of the water-water correlations also helps to establish strong alignment of water dipoles along local electric fields of the ionized surface residues. Water dipoles between these strongly orientated domains are frustrated, i.e., they do not have a strong orientational preference and are mostly disordered orientationally [74]. Several observables related to dipolar orientations show somewhat unusual and long-ranged decay of the interfacial perturbation into the bulk [77, 78]. On the other hand, the density correlations do not propagate beyond the first hydration layer, which suggests that only the orientational manifold is responsible for a long-range perturbation of the water structure. In other words, if any "biological water" exists around proteins, it can manifest itself only in the orientational structure and not in an extended density profile of the hydration shell [79].

The distinction between the orientational and density structure of the hydration shell is seen from the temperature dependence of the corresponding susceptibilities (figures 9 and 10). The dipolar susceptibility of the shell can be defined by the following relation

$$\chi_M(a) = \frac{1}{3k_{\mathrm{B}}Tv_w}\frac{\langle \delta M_s(a,0)^2\rangle}{\langle N_s(a)\rangle} \tag{26}$$

Here, $\mathbf{M}_s(a,t)$ is the instantaneous dipole moment of the shell of thickness a and

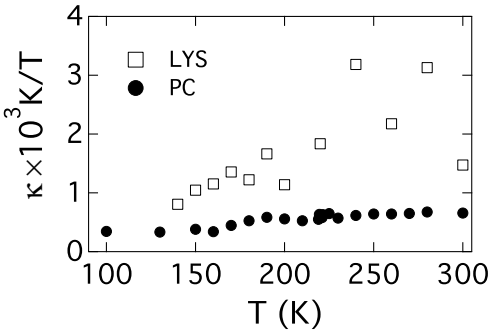

Figure 10: Compressibility of the first hydration shell ($a \simeq 3$ Å) multiplied with $10^3\mathrm{K}/T$. The results are from MD simulations of plastocyanin (PC) [81] and lysozyme (LYS) [74] vs temperature. Adapted with permission from [74]. Copyright 2015 American Chemical Society.

$\delta\mathbf{M}_s(a,t)$ is the fluctuation. In addition, $v_w = (\pi/6)\sigma_w^3$, $\sigma_w = 2.87$ Å is the volume of a single water molecule and $N_s(a)$ is the fluctuating number of water molecules in the shell. Density fluctuations can be characterized by the shell compressibility [80]

$$\kappa(a) = \langle \delta N_s(a)^2 \rangle / \langle N_s(a) \rangle. \tag{27}$$

It should saturate to the bulk limit $\kappa(\infty) = k_\mathrm{B} T \rho \beta_T$ expressed through the isothermal compressibility β_T and the number density of bulk water ρ. This relation is another case of the Nyquist theorem predicting that the variance of the number of shell waters should be proportional to temperature. Therefore, in analogy with $\chi_M(a)$, figure 10 shows the dependence of $\kappa(a,T)/T$ on T at $a \simeq 3$ Å.

The comparison of figures 9 and 10 clearly shows that dipolar and density susceptibilities change oppositely with increasing temperature. The increase of the dipolar susceptibility with cooling is particularly interesting. The sharp drop of χ_M at $T \simeq 160$ K (lysozyme) is identified with the glass transition of the protein [82]. A higher turnover temperature for plastocyanin in figure 9 is related to a shorter simulation time [73]. The real part of the shell dipolar susceptibility $\chi'_M(\omega)$ calculated at frequency ω shows a more rounded maximum vs T, which shifts to higher temperatures with increasing ω. This general phenomenology is well established for bulk relaxor ferroelectrics [83]. These materials display a number of properties attributed to cooperative dipolar nanodomains. Random charge impurities are responsible for their formation, and they are prevented by disorder from forming a regular ferroelectric crystal. The dielectric constant of a relaxor ferroelectric increases with lowering temperature. It, however, does not reach the Curie point of the ferroelectric transition, but instead drops at a glass-transition temperature when dipolar domains dynamically freeze on the time of observation.

An analogy to the protein-water interface cannot be missed here. Proteins are characterized by a nearly uniform distribution of the surface charge [84]. The oppositely charged surface residues create random pinning sites for the interfacial water molecules.

They both preferentially orient the water dipoles in each domain and prevent the domains growth beyond the size restricted by the average distance between the opposite charges. Whether the uniform distribution of the protein surface charge has evolved to avoid the growth of the dipolar nanodomains is not known. However, their existence has a direct relation to the problem of electron transfer and biochemical reactivity because they enhance the magnitude of the electrostatic noise sensed by the protein active sites. We now turn to the question of how the properties of the protein-water interface are projected onto the statistics and dynamics of the reaction coordinate X.

6. Physical interactions

In the electron-transfer formalism, the specific structure of the protein-water interface is projected on one collective coordinate, the donor-acceptor energy gap (figure 2) [31]. This single coordinate absorbs the entire manifold of nuclear degrees of freedom affecting the energy levels of the transferred electron. As we discuss in more detail below, the resulting statistics of X incorporates not only the interaction energies of the donor and acceptor sites with the surrounding medium, but also the entropies related to the number of microscopic states required to achieve a particular value of X and restrictions on the number of microscopic states imposed by nonergodicity. Here we give a somewhat simplified description of the interactions primarily contributing to the observable parameters of the electron transfer kinetics, the average energy gap $\langle X\rangle$ and the variance σ_X^2 (equation 2).

The main contributor to X is the Coulomb interactions of the donor and acceptor charges with the atomic charges of the thermal bath [85, 32]. Correspondingly, the Coulomb component of the energy gap is $X^{\rm C}=\sum_j \Delta q_j\phi_j$, where the sum runs over the partial charges of the donor and acceptor atoms altered by electron transfer to produce the difference charges $\Delta q_j = q_{2j} - q_{1j}$ between the final, q_{2j}, and initial, q_{1j}, states. Further, ϕ_j is the instantaneous electrostatic potential of the thermal bath at site j of the donor-acceptor complex.

The Coulomb energy gap $X^{\rm C}$ can be viewed as the first-order perturbation, produced by the bath, of the quantum-mechanical eigenenergies of the donor and acceptor electronic states: $X^{\rm C}=\langle\Psi_2|\hat{H}^{\rm C}|\Psi_2\rangle-\langle\Psi_1|\hat{H}^{\rm C}|\Psi_1\rangle$, where Ψ_i are the wave functions in the electron-transfer states and $\hat{H}^{\rm C}$ is the Hamiltonian of the Coulomb interaction. The overall energy gap also contains the gas-phase component X_0. One can next proceed to the second-order perturbation in $\hat{H}^{\rm C}$, which results in the induction solute-bath interaction [86]. If the distribution of the molecular charge of the bath molecules is approximated by the dipole, one arrives at the dipolar polarizability α_k of the bath molecule or a molecular group and the induction component in the instantaneous energy gap [87]

$$X^{\rm ind}=-\tfrac{1}{2}\sum_k \alpha_k\left[E_{2k}^2-E_{1k}^2\right]. \tag{28}$$

Here, E_{ik} $(i=1,2)$ is the magnitude of the electric field created by the donor-acceptor

complex at the molecular group k carrying the polarizability α_k. The total donor-acceptor energy gap can, therefore, be written as $X = X_0 + X_b$, where $X_b = X^{\rm C} + X^{\rm ind}$ accounts for the interactions with the bath.

Coulomb interactions, arising from the first-order perturbation of the electron eigenenergy, are by far strongest interaction of the electron with the bath. The interactions with the negative and positive atomic charges are, however, strongly compensated in the total $X^{\rm C}$. In contrast, induction interactions all carry the same sign and add up in $X^{\rm ind}$. As a result, $\langle X^{\rm ind}\rangle$ is often comparable to $\langle X^{\rm C}\rangle$ [65].

The induction interaction has a classical representation as the free energy of polarizing the induced dipole $p_k = \alpha_k E_{ik}$ [88]. Since induced dipoles adiabatically follow the changes in the charge distribution caused by electron transfer, fluctuations of the induction gap are driven by the density (translational) fluctuations of the medium. In contrast, fluctuations of the Coulomb energy are dominated by orientational motions. The difference in the dominant nuclear modes leads to strongly distinct contributions to the variance of the energy gap, which is dominated by the Coulomb component. This is because the density fluctuations are constrained in the closely packed protein/lipid/water medium, while the orientational fluctuations of molecular multipoles are less hindered and produce more intense fluctuations. The induction part of λ is small compared to the Coulomb component for sufficiently slow reactions. Local density fluctuations tend, however, to be faster than collective orientational fluctuations and the induction part of λ grows in significance for ultra-fast reactions, when the Coulomb part becomes dynamically frozen [65] (see below).

Accurate calculations of the bath energy gap X_b require numerical force-field simulations. Estimates can be done, however, based on plausible models and general solvation susceptibilities [87]. In the case of the induction interactions, one can assume that the surrounding polarizable medium is characterized by a uniform polarizability α of molecular groups distributed with the number density ρ. Such a medium should carry the refractive index n, which can be determined from the Clausius-Mossotti equation, $(n^2-1)/(n^2+2) = (4\pi/3)\rho\alpha$. One next assumes that the donor and acceptor can be represented by spherical cavities with the radii R_D and R_A, respectively (Marcus configuration [4]). They are additionally assumed to carry charges Z_D and Z_A in the initial state, which become $Z_D + 1$ and $Z_A - 1$ after electron transfer. The induction shift becomes

$$\langle X^{\rm ind}\rangle_1 = -3e^2\,(g_1 + g)\,\frac{n^2-1}{n^2+2}, \tag{29}$$

where e is the elementary charge, the geometric parameters are

$$\begin{aligned} g_1 &= \frac{Z_D}{R_D} - \frac{Z_A}{R_A} - \frac{Z_D - Z_A}{R}, \\ g &= \frac{1}{2R_A} + \frac{1}{2R_D} - \frac{1}{R}, \end{aligned} \tag{30}$$

and R is the donor-acceptor distance. For instance, in the case of primary charge separation in bacterial photosynthesis, one has $R_D = R_A = 5.6$ Å and $R = 11.3$

Å. With the typical value of the refractive index of the protein $n = 1.473$, one gets $\langle X^{\rm ind}\rangle_1 = -1.1$ eV with $Z_D = Z_A = 0$, which compares favorably with -1.0 eV from MD simulations [47]. When the same model is applied to the reorganization energy, one gets [89]

$$\lambda^{\rm ind} \simeq \frac{3\beta e^4\sigma^3}{320\eta}\left(\frac{n^2-1}{n^2+2}\right)^2 \kappa g^{\rm ind}, \tag{31}$$

where κ is the shell compressibility given by (27), $\eta = (\pi/6)\rho\sigma^3 \simeq 0.5$ is the medium packing density defined assuming the effective diameter σ of the medium particles, and

$$g^{\rm ind} = \frac{(2Z_D+1)^2}{R_D^5} + \frac{(2Z_A-1)^2}{R_A^5}. \tag{32}$$

With $\kappa = 0.4$ and $\sigma = 4$ Å, one gets for the case of bacterial charge separation $\lambda^{\rm ind} \simeq 0.11$ eV. The value calculated from MD simulations is 0.12 eV [65]. This value should be compared to the overall nonergodic reorganization energy $\lambda(k) \simeq 0.45$ eV, while the reorganization energy from the entire length of the simulation is $\simeq 2$ eV (table 1). This examples quantifies the trend presented in figure 8, where the reorganization energy on the picosecond reaction time is much lower (fraction of eV) compared to the value obtained from the entire 13 μs of simulations.

In order to provide a coarse-grained description of the Coulomb component $X^{\rm C}$, one needs to switch to a set of collective coordinates describing the medium. The dipolar polarization density of the thermal bath $\mathbf{P}(\mathbf{r})$ is a common choice [4] when dealing with polar media. This choice does not exhaust the list of possible collective variables and, for instance, inhomogeneous liquid density around the donor-acceptor complex is another collective variable required for reactions in molecular liquids [90, 91].

When the solvent collective variables are limited by the dipolar polarization field, the donor-acceptor complex couples to this field through its vacuum electric field $\mathbf{E}_i$ [92]. The Gaussian system Hamiltonian is defined by introducing the solvation susceptibility χ

$$H_i[\mathbf{P}] = -\mathbf{E}_i * \mathbf{P} + \frac{1}{2\chi}\mathbf{P} * \mathbf{P}. \tag{33}$$

Here, the asterisks denote both the scalar product and the integration of the fields over the volume occupied by the polar medium. From this equation, the average Coulomb energy gap is obviously $\langle X^{\rm C}\rangle_i = -\chi\Delta\mathbf{E} * \mathbf{E}_i$, where $\Delta\mathbf{E} = \mathbf{E}_2 - \mathbf{E}_1$. When the above model of two spherical cavities with charges Z_D and Z_A is applied, one gets

$$\langle X^{\rm C}\rangle_1 = -4\pi\chi e^2 g_1 \tag{34}$$

and a similar equation for $\langle X^{\rm C}\rangle_2$ (g_1 is given by (30)).

Equation (34) is not typically used in electron transfer theories [4]. Instead, one separates $\mathbf{E}_1$ into the sum of the mean field $\bar{\mathbf{E}} = (\mathbf{E}_1 + \mathbf{E}_2)/2$ and the difference field as follows: $\mathbf{E}_1 = \bar{\mathbf{E}} - \Delta\mathbf{E}/2$. The average energy gap then becomes the sum of the solvent reorganization energy $\lambda = (\chi/2)\Delta\mathbf{E} * \Delta\mathbf{E}$ and the electrostatic solvation free

energy $\Delta F_s = -(\chi/2)\,[\mathbf{E}_2 * \mathbf{E}_2 - \mathbf{E}_1 * \mathbf{E}_1]$: $\langle X^{\rm C}\rangle_1 = \lambda + \Delta F_s$. Further, when ΔF_s is combined with X_0 and $\langle X^{\rm ind}\rangle_1$ into the reaction free energy $\Delta F_0 = X_0 + \langle X^{\rm ind}\rangle_1 + \Delta F_s$, one arrives at the standard representation of the average donor-acceptor energy gap in terms of the reorganization energy and the reaction free energy

$$\langle X\rangle_1 = \lambda + \Delta F_0, \tag{35}$$

as, for instance, in equation (12).

The standard results of the Marcus theory [4] follow from this general Gaussian solvation model by applying the longitudinal solvation susceptibility of a spherical solute with the charge at its center, $\chi = (4\pi)^{-1}c_0$, where the Pekar factor $c_0 = \epsilon_\infty^{-1} - \epsilon_s^{-1}$ is designed to incorporate only the nuclear polarization modes in the response of a dielectric with the static dielectric constant ϵ_s and the high-frequency dielectric constant ϵ_∞. The reorganization energy of the polar medium becomes $\lambda = e^2 c_0 g$, where g is given by (30). One has to keep in mind that the Marcus equation applies only to the specialized case of spherical solutes with centered charges. Any deviation from this geometry or charge distribution will lead to a change of the solvation susceptibility [90]. For instance, it turns into the Onsager expression for the reaction field [93] if the donor-acceptor complex is approximated by a spherical point dipole.

Equation (35) has played an enormous role in the the theory of electron transfer reaction [4] since it allows one to connect the average energy gap to the reaction free energy measured separately. One, however, needs to realize its potential pitfalls since it turns into a mathematically poorly defined construct for some configurations. The simple and conceptually useful case is the charge-separation reaction when $\mathbf{E}_1 = 0$ in the initial state. The average Coulomb energy gap is obviously zero, $\langle X^{\rm C}\rangle_1 = 0$, and only induction solvation contributes to the reaction free energy $\Delta F_0 = X_0 + \langle X^{\rm ind}\rangle_1$. However, the zero value is of the Coulomb energy gap is achieved by complete cancelation of two large Coulomb energies in ΔF_0 and λ in equation (35), with inevitable uncontrollable errors when each component is measured or calculated separately. The case of nonergodic electron transfer common to proteins presents additional complications.

The splitting of the vertical energy gap into the reorganization (free) energy and the reaction free energy is not very useful for nonergodic electron transfer since neither of the two are well-defined as thermodynamic free energies. Keeping the average energy gap in the nominator of the expression for the activation barrier, as in equation (3), is more consistent both conceptually and computationally. Alternatively, one can use $\lambda(k) + \Delta F(k)$ in equation (35), but the advantage of a separate input of the thermodynamic reaction free energy, such as from equilibrium electrode potentials, is lost here. The nonergodic free energy might still be a useful concept as a gauge of the system nonergodicity. The detailed balance is still valid for nonergodic kinetics and the ratio of the forward to backward rates gives access to $\Delta F(k)$. This value can be compared to the thermodynamic ΔF_0 from redox potentials.

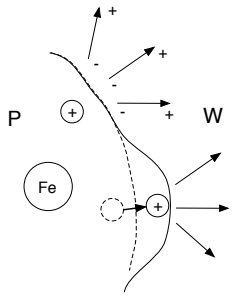

Figure 11: Illustration of the charge distribution at the protein-water interface. The active site is represented by the iron atom of the heme cofactor. A positively charged residue of the protein (P) creates a positive electrostatic potential at the iron. The water (W) dipoles polarized by the same residue produce an average potential opposite in sign to the potential of the charged residue. An elastic deformation of of the protein moves the charged residue, and the water dipoles of the polarized interfacial nanodomain follow that displacement adiabatically.

7. Protein and water components of the thermal bath

Cross-membrane electron transport proceeds in a highly heterogeneous environment involving protein, water, lipids, and ions in the solution. However, the protein and its hydration shells are main contributors to the fluctuations of the energy gap. More specifically, concerted fluctuations of the protein-water interface is what dominates the high magnitude of electrostatic fluctuations at the active sites. This feature makes hydrated protein a unique "fluctuation machine" and deserves special discussion.

The donor-acceptor energy gap can be separated into component contributions. Keeping the protein and water as two main components, one writes for the bath energy gap $X_b = X_p + X_w$, where "p" and "w" stand for the protein and water, respectively. It turns out that $\langle X_p \rangle$ and $\langle X_w \rangle$ often carry opposites signs [42]. Looking at the electrostatics of the protein and water helps to explain this result. To simplify the problem, one can consider the electrostatic potential of the medium created at a given site within the protein.

Figure 11 explains the origin of the opposite signs of the protein and water potentials from the viewpoint of the distribution of charge at the protein-water interface. Assume that the site of interest is the iron of the heme cofactor within the protein matrix. One can next consider a positively charged residue at the interface, which will produce a positive potential at the iron site. However, that positive residue will polarize the closest waters in a way of creating an effective negative charge density at the protein-water dividing surface. The average potential created by water at the iron site will be opposite in sign to the potential of the surface residue thus screening it. Figure 12 details this qualitative conclusion by showing the distribution of the protein and water electrostatic potentials producing averages of opposite sign.

We next consider what happens when the protein and water contributions are combined to produce λ. As is seen from figure 8, they are both substantial, but also do not add up to the overall λ. The reason is the cross term: the reorganization energy

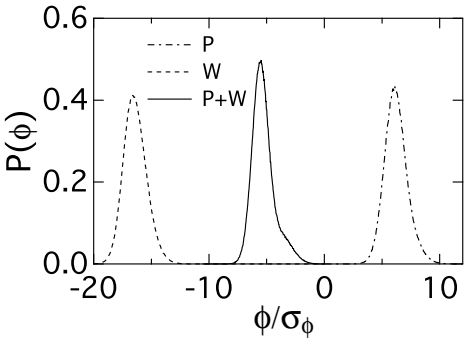

Figure 12: Distribution of the electrostatic potential ϕ at the iron of the heme of the reduced form of cytochrome c produced by the protein (P), water (W), and protein and water combined (P+W) [42]. The distribution function $P(\phi)$ is plotted against the potential normalized by its variance $\sigma_\phi = \langle(\delta\phi)^2\rangle^{1/2}$. Adapted with permission from [42]. Copyright 2011 American Chemical Society.

can be written as the sum of individual protein and water components and a cross term originating from cross-correlations between X_p and X_w: $\lambda = \lambda_p + \lambda_w + \lambda_{pw}$. The mutual screening of protein and water electrostatics makes λ_{pw} negative (e.g., $\lambda_w > \lambda$ in figure 8), often significantly compensating large individual contributions from the protein and water separately. Despite this mutual compensation, λ is still large. It turns out that many unusual properties of the protein-water interface come into focus in an attempt to understand this result.

Figure 11 provides a general understanding of the origin of large-scale interfacial fluctuations gauged by λ. Protein is an elastic polymer capable of elastic deformations of its global folded shape [94]. Elastic deformations require time-scales significantly longer than those of intramolecular vibrations, in the range of a few nanoseconds [95]. These motions produce high-amplitude displacements of the charged surface residues and of the surface water domains strongly polarized by them. Both effects contribute to intense fluctuations of the electrostatic potential at the protein active site. The concerted character of the protein and water fluctuations is seen in the loss function as a common relaxation process at $\omega \sim 1$ ns^{-1} [42, 96] (figure 13). This process is universally observed in simulations of hydrated proteins, with a shift to lower relaxation frequencies when the size of the protein is increased [40].

A consistent physical picture emerges from these observations. The destruction of the bulk water structure and the creation of interfacial dipolar nanodomains combine with elastic fluctuations of the protein shape to produce intense electrostatic fluctuations at the active sites. Importantly, these fluctuations contribute most significantly to the large magnitude of λ. The cross protein-water term λ_{pw} is strongly affected by the distribution of protein's surface charge [42] and can significantly lower the overall magnitude of λ. It is also decreased by freezing protein's elasticity by either decreasing the temperature below the protein dynamical/glass transition (see below) or by imposing restraining forces on the protein motions in the course of simulations [81]. Figure 14

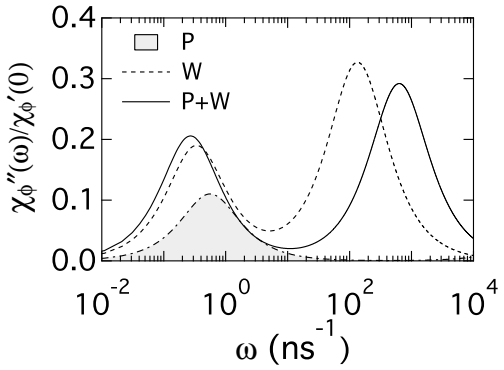

Figure 13: The normalized loss function $\chi''_\phi(\omega)/\chi'_\phi(0)$ of the electrostatic potential at the heme iron of reduced cytochrome c protein [42]. The total loss function (P+W) is separated into the protein (P) and water (W) components. Adapted with permission from [42]. Copyright 2011 American Chemical Society.

illustrates this general result. With lowering the temperature one reaches the point when elastic deformations become dynamically frozen on the instrumental/simulation observation window. Only fast localized modes can equilibrate at lower temperatures and the system effectively behaves as a bath of harmonic oscillators with $\lambda^{\rm St} \simeq \lambda$ [81]. The prediction of the fluctuation-dissipation theorem is restored at these low temperatures. The value of $\lambda \simeq 0.7 - 0.8$ eV for this elastically frozen protein is consistent with the expectation from a model considering polar bulk water in contact with a non-polar protein core.

8. Non-Arrhenius rate law

The Arrhenius law assumes that the free energy of activation is temperature independent. For electron transfer driven by Gaussian nuclear modes, this requirement implies two statements: the average gap $\langle X \rangle$ is temperature-independent and the gap variance σ_X^2 is proportional to temperature (equation (7)). Both the average energy gap and its variance are calculated as statistical averages over the canonical or dynamically restricted ensembles with the weight of each point in the phase space given by $\rho(\Gamma)d\Gamma_k$. This complete description is difficult to implement for complex systems and the preference is often given to statistical averages taken over just a few collective coordinates coupled to the donor-acceptor energy gap.

When the description is shifted from the phase space Γ or Γ_k to just a few collective coordinates $Q = \{Q_i\}$, the weight of each configuration in the space of coordinates Q_i is determined by the free energy instead of the Hamiltonian

$$\rho(\Gamma)d\Gamma_k \to e^{-\beta F(Q)} \prod_{\omega>k} dQ_{\omega,i}. \tag{36}$$

The consequence of this reduction of the phase space is that one gets the number of microscopic states corresponding to a given set of Q_i as an entropic part $S(Q)$

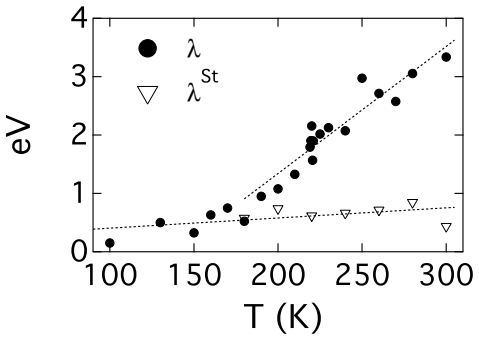

Figure 14: Temperature dependence of λ and λ^{St} of plastocyanin in TIP3P water from MD simulations [81]. The dotted lines are linear regressions drawn through the points to guide the eye.

of $F(Q)$. The probability of a given fluctuation of the collective modes is defined not only by the corresponding energy penalty, but also by the change in the number of microscopic states. This perspective allows one to understand possible origins of the temperature dependence of the activation barrier and the appearance of the non-Arrhenius temperature law for the reaction rate.

If the fluctuations near the equilibrium are small, one can always expand the energy part of the free energy $F(Q)$ near the equilibrium positions Q_{0i}

$$F(Q) = -TS(Q) + \sum_i \frac{k_i}{2}(Q_i - Q_{0i})^2. \tag{37}$$

Here, k_i are the force constants of harmonic displacements from the equilibrium. One can now calculate the first and second moments of the donor-acceptor energy gap $\Delta E(Q)$ by using equations (15) and (16)

$$\langle \dots \rangle = (Z'_k)^{-1} \int \dots e^{-\beta F(Q)} \prod_{\omega>k} dQ_{\omega,i}, \tag{38}$$

where $Z'_k = \int \exp[-\beta F(Q)] \prod_{\omega>k} dQ_{\omega,i}$. The calculation of this integral is complicated by the generally unknown entropy term $S(Q)$ in equation (36). However, if the energy is the dominant part of $F(Q)$, the result is straightforward. For $X(Q)$ approximated by a linear function of Q, one obtains a temperature-independent average energy gap $\langle X \rangle$ and the variance proportional to temperature $\sigma_X^2 \propto T$ (Nyquist theorem). This is the case when the Arrhenius law strictly holds. Any situation that involves an entropic component $S(Q)$ in (36) will produce some kind of temperature dependence of the activation barrier deviating from the strictly harmonic result. How strong such deviations might be is hard to determine for a system as complex as a hydrated protein. Answering this question is greatly helped by MD simulations carried out at different temperatures [81, 96].

Figure 15 shows $\sigma_X(T)^2$ obtained from MD simulations of two proteins, plastocyanin [81] and a green fluorescent protein (GFP) [96]. In the first case, the

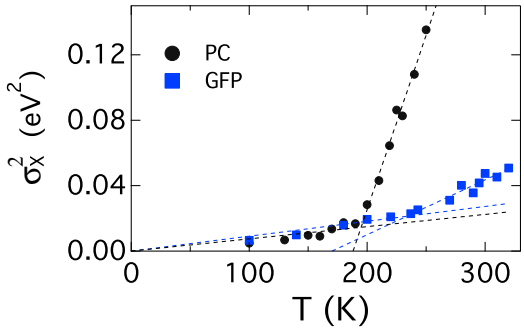

Figure 15: Temperature dependence of σ_X^2 obtained from MD simulations of plastocyanin (PC) [81] and green fluorescent protein (GFP) [96]. The dashed lines are linear fits through the high-temperature and low temperature portions of the data. The low-temperature points are fitted to $\sigma_X^2 \propto T$, while the high-temperature points are fitted to $\sigma_X^2 \propto (T - T_0)$; $T_0 = 170$ K for GFP and $T_0 = 188$ K for PC.

half redox reaction [97] of changing the redox state of the copper active site is studied, while in the second case the change of the charge distribution of the active site is caused by an optical excitation. In both cases, $\sigma_X(T)^2$ is more complex than the harmonic prediction, $\sigma_X(T)^2 \propto T$. The overall temperature dependence follows two approximately linear regimes, changing slope at a cross-over temperature. The temperature at which the slope breaks is in the range of values typically assigned to the dynamical transition in proteins [17, 98]. Clearly, the high-temperature part of $\sigma_X(T)^2$ is of main interest since it determines the temperature dependence of the rate constant in the physiological range of temperatures. It is approximately given by a linear function of temperature, with an offset T_0

$$\sigma_X(T)^2 \propto (T - T_0). \tag{39}$$

When substituted into equation (3), this function leads to the Vogel-Fulcher-Tammann (VFT) form of the rate constant often reported for relaxation and viscosity of fragile glass-formers [16]

$$k \propto \exp\left[-\frac{AT_0}{T - T_0}\right]. \tag{40}$$

Here, A is a temperature-independent constant. Note also that the low-temperature portion of the simulation data follows the harmonic behavior, $\sigma_X(T)^2 \propto T$.

Both the linear, with a non-zero offset, form of σ_X^2 and the VFT law for the relaxation rates are empirical observations. However, the VFT law provides quite an accurate representation of the dynamics of a large class of super-cooled liquids [16, 99], and its appearance in the kinetics of protein electron transfer must have a physical justification. On the qualitative level, it must be related to the manifold of microstates of the protein achievable for a subset of collective modes Q_i, which are further projected on the single reaction coordinate X. The enormous reduction of the configuration space to just one reaction coordinate X must result in a significant entropic component

in the free energy surface of electron transfer. A complex temperature dependence of the Gaussian width σ_X^2, obviously violating the simple Nyquist prescription, is a manifestation of this physical reality testable by laboratory measurements. We next show that the entropic component of the free energy barrier is related to the skewness (non-parabolicity) of the free energy surfaces.

9. Non-Gaussian statistics

The question of whether the Gaussian statistics of the energy gap leading to parabolic free energy surfaces applies to donor-acceptor molecules dissolved in dense molecular media has a long history [100, 101, 102, 103]. Most evidence suggests that the statistics of X is Gaussian [102] when electrostatic interactions between the charge-transfer complex and the medium are considered. Non-Gaussian distributions appear even in simple systems when quadratic solute-solvent coupling, for instance due to solute's polarizability, is allowed [104]. The situation for biological macromolecules has not been studied.

Understanding of potential non-Gaussian effects in electron transfer has been significantly hampered by both the requirement of enhanced sampling at the wings of the distribution and the need to come up with model free energy functions satisfying the linear relation in equation (6). The latter constraint is particularly stringent since it requires essentially exact analytical solutions for both free energy surfaces, which are available for very few theoretical models [104]. However, if the requirement of the linear relation is lifted in an approximate model, the extent of deviation from the Gaussian statistics of a single free energy surface can be estimated from either the higher moments or from the temperature dependence of the lower moments. Since even second moments of X are often challenging to calculate from simulations of proteins [105], the second route seems to be more reliable at the present level of computational capabilities.

One can start with the standard definition of the nth order central moment

$$\langle \delta x^n \rangle = Z_X^{-1} \int (\delta x)^n e^{-\beta F(x)} dx, \tag{41}$$

where $Z_X = \int \exp[-\beta F(x)] dx$ and the index specifying the electron-transfer state has been dropped for brevity. We are also using the dimensionless variable $x = X/\sigma_X$ to simplify the derivation. From this equation one can directly derive the relations for the third and fourth central moments in terms of the temperature derivatives of the corresponding lower moments

$$\begin{aligned} \langle \delta x^3 \rangle &= \frac{2}{\sigma_X} \frac{\partial \langle X \rangle}{\partial \ln T}, \\ \langle \delta x^4 \rangle &= 1 + 2 \frac{\partial \ln \sigma_X^2}{\partial \ln T}. \end{aligned} \tag{42}$$

Derivation of these equations requires estimating the moments such as $\langle \delta x \delta F \rangle$. We neglected here the non-harmonic corrections to $F(x)$ and used $\beta F(x) \simeq \beta F_0 + \delta x^2/2$ (equation (8)) in estimating such correlations.

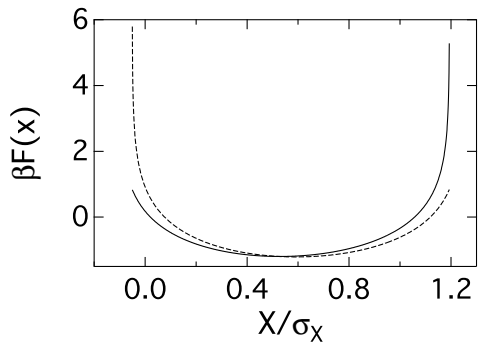

Figure 16: $\beta F(x) = -\ln[P(x)]$ vs $x = X/\sigma_X$ for GFP protein in its ground state [96]. The probability $P(x)$ is calculated from equation (43) truncated at $n > 3$ (dashed line) and $n > 4$ (solid line). The series coefficients in (43) are evaluated from the temperature derivatives of the first and second moment according to (42).

The central moments can be used to estimate deviations from the Gaussian distribution using the method of Zernicke [106]. The non-Gaussian distribution function is given in this approach by a series of Hermite polynomials $H_n(x)$

$$P(x) = (2\pi)^{-1/2} e^{-x^2/2} \sum_{n=0}^{\infty} C_n H_n(x) \tag{43}$$

in which $C_0 = 1$ and the non-zero terms in the expansion start from C_3.

The prescription given by equations (42) and (43) was used to estimate the non-Gaussian effects by including only $C_3 = \langle \delta x^3 \rangle / 3!$ and $C_4 = (\langle \delta x^4 \rangle - 3)/4!$ in the series of Hermite polynomials. The temperature derivation of the ground-state GFP is used to produce the corresponding free energy surface $\beta F(x) = -\ln[P(x)]$. The use of the temperature slopes of $\langle x \rangle$ and σ_X^2 from MD simulations [96] (figure 15 for σ_X^2) results is $\langle \delta x^3 \rangle = -9.9$ and $\langle \delta x^4 \rangle = 5.2$ ($\langle \delta x^3 \rangle = 0$ and $\langle \delta x^4 \rangle = 3$ for the Gaussian statistics). The resulting free energy surface is shown in figure 16. The skewness resulting from a large third central moment shifts the minimum of the free energy surface off the zero position. In addition, the shape of the curve shows a flat bottom, consistent with a large λ produced by the simulations of GFP [96], and steep non-Gaussian wings of the distribution. It still remains to be seen how estimates of this type compare to direct sampling of the free energy surfaces by numerical simulations.

In terms of experimental observations, measurements of the temperature dependence of the reaction rates gives access to some of the parameters discussed here. For instance, the activation enthalpy, $H^{\mathrm{act}} = \partial(\beta F^{\mathrm{act}})/\partial\beta$ becomes

$$\beta H^{\mathrm{act}} = \tfrac{1}{4}\langle x \rangle^2 \left(\langle \delta x^4 \rangle - 1 \right) - \tfrac{1}{2} \langle x \rangle \langle \delta x^3 \rangle. \tag{44}$$

This expression can be converted into the relation between H^{act}, F^{act} and the two higher moments given that $\beta F^{\mathrm{act}} = \langle x \rangle^2/2$. If the skewness is the main contributor to the non-Gaussian statistics, which is the case with GFP in figure 16, one can arrive at a simple

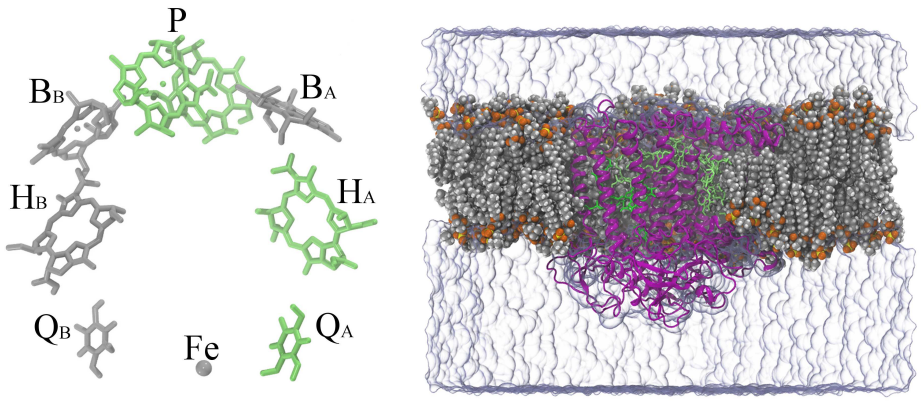

Figure 17: Left Panel: Schematic arrangement of cofactors in the bacterial reaction center. The primary electron donor (P), bacteriopheophytin (H_A), and quinone molecule (Q_A) are colored in green; the corresponding cofactors of the inactive branch, the monomer bacteriochlorophyll (B_A), and the non-heme iron are shown in grey. Electron transfer in wild-type reaction centers occurs almost exclusively along the A-branch of cofactors (subscript "A"), while the B-branch (subscript "B") is mostly inactive. Right panel: MD simulation setup showing the reaction center in the bilipid membrane: the water is represented as a transparent surface, the lipid membrane is rendered in a van der Waals representation, the protein is shown in purple, and the cofactors are rendered as green licorice bonds.

equation for it in terms of the activation free energy and activation enthalpy

$$H^{\rm act} = F^{\rm act} - \sqrt{F^{\rm act}/(2\beta)}\langle \delta x^3 \rangle. \tag{45}$$

From this relation, the entropy of activation $TS^{\rm act} = H^{\rm act} - F^{\rm act}$ becomes a direct measure of the skewness of the distribution of the donor-acceptor energy gap.

An additional source of activation parameters can be provided by electrochemical measurements, which allow one to modulate $\langle x \rangle$ with the electrode overpotential η: $\langle x \rangle \to \langle x \rangle + e\eta/\sigma_X$, e is the elementary charge. The transfer coefficient, $\alpha = \partial F^{\rm act}/\partial(e\eta)$, often available from electrochemistry [6], puts an additional constraint on the values of the first and second moments, $\alpha = \langle x \rangle/(\beta\sigma_X)$. We also note that $\langle X \rangle$ and σ_X^2 correspond to, respectively, the maximum and the Gaussian inhomogeneous width of an optical band of a photoexcited electronic transitions [107]. Therefore, optical thermochromism (measuring optical band-shapes as a function of temperature) gives access to higher spectral moments according to equation (42).

10. Bacterial Photosynthesis

The general mechanistic principles of electron transfer discussed above fully apply to reaction steps of electron transport in reaction centers of bacterial photosynthesis [3, 9]. The separate steps in this cross-membrane electron transport occur on the time-scales from picoseconds to milliseconds. Each step is affected by a different subset of protein's nuclear modes and the use of the nonergodic kinetics becomes essential. If a simple

Table 1: Reorganization energy $\lambda = (\lambda_1 + \lambda_2)/2$ determined as the mean of the reorganization energies for the forward (1) and backward (2) reactions and measured from the variance of the donor-acceptor energy gap on the simulation trajectory (equation 7). Also listed are the Stokes-shift reorganization energy λ^{St} and the ratio $\kappa_G = \lambda/\lambda^{\mathrm{St}}$ [108, 40]. P^* denotes the photoexcited primary pair, while P stands for its ground state.

Reaction	λ	λ^{St}	κ_G
$\mathrm{P}^*\mathrm{B_A} \leftrightarrow \mathrm{P}^+\mathrm{B_A^-}$	2.03	0.77	2.6
$\mathrm{B_A^-H_A} \leftrightarrow \mathrm{B_AH_A^-}$	2.24	0.71	3.2
$\mathrm{PH_A} \leftrightarrow \mathrm{P}^+\mathrm{H_A^-}$	2.55	0.89	2.9
$\mathrm{H_A^-Q_A} \leftrightarrow \mathrm{H_AQ_A^-}$	1.83	1.10	1.7

conclusion can be drawn from our calculations of individual electron-transfer rates in the bacterial reaction center, it would be the realization that the traditional Marcus picture of electron transfer [4] is inapplicable here [40, 47, 65, 108].

Figure 17 shows the electron transfer pathway through a sequence of cofactors located in the membrane-bound reaction center. Light is absorbed by a bacteriochlorophyll dimer (P), and the electron is transferred via a monomer bacteriochlorophyll ($\mathrm{B_A}$) to a bacteriopheophytin ($\mathrm{H_A}$) in a few picoseconds. This primary charge separation is followed by a 200 ps electron transfer to the first of two quinones ($\mathrm{Q_A}$) and, finally, to a second quinone ($\mathrm{Q_B}$) in 200 μs. The back reactions of each step are 2–4 orders of magnitude slower than the forward reactions, resulting in a quantum yield near unity [9]. Since the reaction is initiated by light, detailed kinetic measurements are possible. As a result of several decades of experimental studies, many of the reaction steps have been studied, also in terms of the dependence of the rates on temperature, protein mutations, etc [109]. We do not review this extensive literature here, focusing instead on whether nonergodic conformational quenching of the protein (figure 5), requiring two separate reorganization energies, is consistent with the existing data. Table 1 summarizes the reorganization energies of individual electron-transfer steps calculated from MD simulations. The results of the simulations were also used to calculate the rates of electron transfer and their temperature dependencies when the corresponding data are available [40, 47, 108]. The theoretical calculations are generally consistent with experiment.

The reorganization energies produced on the length of the simulation trajectory indicate that the protein is trapped in the conformationally quenched state on the simulation time-scale of 10–100 ns insufficient to explore all possible conformations consistent with a given redox states. This is reflected by $\kappa_G > 1$ found for all reactions in the reaction center (table 1). This state of the protein corresponds to the discontinuous ergodicity breaking.

The forward electron-transfer steps are in the normal region of electron transfer where intramolecular vibrations are not effective [5]. The nonergodic reaction rate can

be obtained by iteratively solving a fairly simple equation (cf. to equation (4))

$$k = \frac{2\pi}{\hbar} V^2 g(k). \tag{46}$$

Here, $g(k)$ is a Gaussian probability of reaching the $X = 0$ activated state. It depends on the rate constant k through $\lambda(k)$

$$g(k) = [4\pi k_{\rm B} T \lambda(k)]^{-1/2} \exp\left[-\frac{\langle X \rangle^2}{4k_{\rm B} T \lambda(k)}\right]. \tag{47}$$

In practice, one starts with an initial guess of $\lambda(k)$, for instance with $\lambda(0)$, on the left-hand side of (47). This guess yields the first iteration k_1 in (46), which is substituted back into $\lambda(k)$ in (47) to continue the cycle until converged. This procedure was used in the calculations based on the loss spectrum of the donor-acceptor energy gap presented in figure 4. The results are generally consistent with experiment, including the energy gap law, i.e., the variation of the rate constant with chemical changes of the cofactors [40, 65].

11. Why are enzymes big?

The mechanism of dynamical control of the reaction by constraining the phase space accessible to the protein motions brings up the question of design principles of natural enzymes [110]. A long-standing inquiry in this field is the reason for large size of protein complexes holding active sites at which catalysis of chemical reaction occurs. The analysis of the protein structure database shows that about 20-40 amino acids are sufficient to make a polypeptide fold into a unique secondary structure. All known enzymes are, however, significantly larger, in the range of 200–800 amino acids [111], and significantly exceed in size both the substrates and the active site, which typically represents about 5% of the enzyme structure. Needless to say that synthesis of these large proteins is energetically costly for the living cell and large proteins must carry some mechanistic advantages for the catalysis.

The dynamical modulation of the chemical activation barrier advocated here offers a possible solution. The control of the kinetics can be accomplished by establishing dynamical resonances between the rate of the reaction and the frequency of a relaxation process affecting the reaction coordinate, $k \simeq \omega_j = \tau_j^{-1}$. In other words, the best tuning of the rate is achieved when the rate constant coincides with a peak in the loss function shown in figure 4. This concept also implies that a significant intensity of the relaxation component should exist on the time-scale of the reaction. Since the rates of many catalytic reactions fall in the range of μs-ms, the enzyme should possess relaxation modes in the same range of frequencies. The most intense electrostatic fluctuations are created by elastic deformations moving protein's ionized surface residues and polarized interfacial water. Therefore, creating resonances between frequencies of elastic deformations with the rate of the reaction requires large proteins, in line with the typical large size of enzymes.

The potential importance of dynamical resonances between reaction rates and relaxation spectra also opens additional possibilities for allostery without conformational change proposed by Cooper and Dryden [112]. The general phenomenon of allostery implies changes in the binding or catalytic ability at an active site imposed by binding of a ligand (effector) at a location distant from the active site [113]. The traditionally accepted view of the allosteric action requires changes in the conformational state upon ligand binding [46], i.e., stereochemical structural change of the protein. In contrast to this view, the idea behind the dynamic allostery of Cooper and Dryden is that altering the spectrum of the protein normal modes affects the Gibbs energy of either the second ligand binding or of the active-site reaction. This view, however, does not involve dynamics and is in reality entropic [114] since "conformational dynamics" in this case stands as a proxy for conformational entropy [112]. The required thermodynamic change is achieved through the alteration of the enzyme's vibrational density of state $g(\omega)$ such that it causes an entropy change $\Delta S \propto \sum_n \Omega_n \Delta g(\Omega_n)$ between the state of bound and unbound effector. One also has keep in mind that the actual allosteric effect consists in altering the reaction/binding entropy at the active site, which requires not just ΔS, but $\Delta\Delta S$ to be significant [112].

The true dynamics of the protein, as for instance recorded by time-resolved fluorescence spectroscopy [115], is not a part of the argument given by the dynamic allostery and conformatinal dynamics views. Ergodicity breaking, and related to it nonergodic activated kinetics, can potentially break the lock of thermodynamics and present arguments in favor of functional dynamics, i.e., a direct connection between truly time-dependent properties of biological macromolecules and their function as catalysts, signal transducers, etc. The restriction of the phase space available to a system on a given observation time affects any calculation of the relevant free energy. Electrostatics affects activation barrier and the corresponding electrostatic solvation energy is relevant here [116]. Similarly to equation (17) for the reorganization energy, the electrostatic solvation energy appears in the restricted ensemble as an integral of the relevant loss function over the range of frequencies exceeding the reaction rate

$$-\Delta F(k) \propto \int_k^\infty \chi''(\omega)\,(d\omega/\omega)\,. \tag{48}$$

This argument becomes clear when applied to the shifted harmonic oscillator in (33). An activation barrier depending on k will follow, with the reaction rate determined from the self-consistent equation (25) of the nonergodic kinetics. The free energy $\Delta F(k)$ is most affected by the dynamics, and the dynamical tuning is most efficient, at the conditions of dynamic resonances. This perspective is universal and applies equally well to both structured and disordered (such as intrinsically disordered proteins) systems. It does not require well-established structures of the traditional theories of allostery operating in terms of conformational changes [114]. However, definitive data connecting slow elastic modes with slow reactions are limited so far to electron transport enzymes [40, 44, 117], which are also known to form particularly large enzymetic complexes belonging to energy chains of photosynthesis and respiration [3].

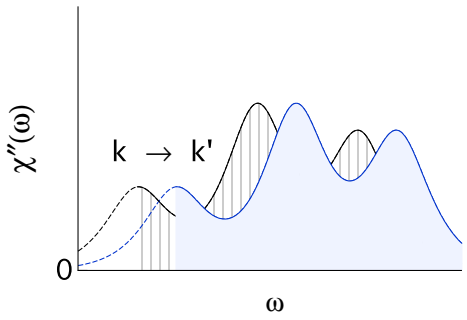

Figure 18: Illustration of the alteration of the loss spectrum caused by binding the effector. The rate constant enters as the lower integration limit in the definition of the activation free energy barrier, as in equation (48). It is then self-consistently determined from the loss spectrum according to equation 23. When the loss spectrum shifts upon binding, the rate constant shifts with the spectrum from the non-bound, k, to the bound, k', value. The acceleration of the catalytic reaction follows from this picture.

A simplified example illustrating a potential scenario is shown in figure 18. Assume that binding the effector globally stiffens the protein and shifts equally all relaxation peaks of $\chi''(\omega)$ to higher frequencies, without changing their relative wights or the protein conformation. The rate constant is self-consistently determined by the relaxation spectrum through equation (25) and is a functional of the loss spectrum. The shift of the entire spectrum to higher frequencies will self-consistently shift the rate constant to a higher value and will speed up the catalysis.

12. Prospectus: dynamics, interfaces, and processing of information

The theory outlined here aims to reexamine the conceptual framework of equilibrium thermodynamics and (Gibbs) free energy in application to production of energy by biology. The power of the concept of equilibrium free energy is in quantifying the "free" (in contrast to "bound") energy available to produce work and to be converted from one form to another. This is the reason why this concept is so indispensable in molecular science where energy is often stored in and released from chemical bonds. The equilibrium free energy combines the average energy and the spread of the system in the phase space (entropy) given in terms of the number of available microstates W

$$F = \langle E \rangle - k_{\mathrm{B}} T \ln W. \tag{49}$$

Both the average energy and the number of microstates are affected by the ability of the system to reach its different configurations. In the Gibbs ensemble, each configuration is assigned the Boltzmann probability p_i such that $\ln W = -\sum_i p_i \ln p_i$ is equal to the Shannon entropy [118].

The requirement encountered in any realistic calculation of the free energy is to sample the phase space on a finite time-scale available to observation. The limited

observation time $\tau_{\rm obs}$, in contrast to $\tau_{\rm obs} \to \infty$ of equilibrium thermodynamics, creates a possibility of ergodicity breaking expressed by constraints, imposed by kinetics, on the part of the phase space available for sampling. The free energy available for work and storage changes to its nonequilibrium value [119]

$$F(k) = \langle E \rangle_k - k_{\rm B}T \ln W_k, \tag{50}$$

where now both the average energy and the number of microscopic states available to the system are constrained by the configurations that can be reached on the observation time-scale $\tau_{\rm obs} = k^{-1}$ (dynamically restricted ensemble). In other words, the free energy of a dynamical system is not only what is available in principle, but to a great extent what can be gained within the schedule. The information about the "schedule", i.e., about the distribution of relaxation times of the medium makes a restricted ensemble essentially a Maxwell's demon [120] trading the information for the reduction of the entropy from $\ln W$ to $\ln W_k$.

The physical information residing inside a system can be associated with either a set of constraints or obtained from measurement [120, 121]. It is the former, that is the constrains imposed by the dynamically restricted ensemble, that are responsible for the information content $I \propto \ln(W/W_k)$. The number of microstates W is the measure of our ignorance about the microstates of a system subjected to macroscopic measurements under a given set of macroscopic constrains [121]. The dynamical control of the ensemble reduces the extent of ignorance by constraining W to W_k and allowing a better control over the evolution of microstates. When applied to the operation of enzymes, which function as processors of information on the cellular level [2, 122], restricted ensembles combine the structural information of a folded macromolecule (enzyme) with its dynamic information into the overall information content of the enzyme catalysis. In this framework, allosteric binding of a ligand discussed above acts to shrink the phase space available to the enzyme. It is then equivalent to the entropy transfer from the enzyme to the heat reservoir.

The energetics of any statistical system obtained from statistical averages over the dynamically restricted ensemble becomes influenced by the match between the $\tau_{\rm obs}$ and the relaxation spectrum τ_j of the medium modes coupled to the reaction coordinate. The problem at hands partially loses the attractive universality of equilibrium thermodynamics, but also introduces new control knobs to optimize the system performance by adjusting the dynamical parameters. The question addressed in this article is whether there is compelling evidence that natural systems are using these additional dynamical controls to improve and optimize their performance. From the limited set of studies focused on electron transport chains made of membrane-bound protein complexes, the answer to this question is affirmative. From a broader perspective, the free energy is too restrictive as the sole predictor of the direction of biological processes. Kinetic and dynamic variables provide additional controls of biological function and optimization through altering the statistical averages and changing the barriers of activated transitions.

Dynamical regulations available within the general concept of nonergodicity will affect different aspects of biology on the molecular and potentially supramolecular level. Nonergodicity eliminates the connection between the first and second statistical moment prescribed by the fluctuation-dissipation theorem. For the mechanistic properties of electron transfer, this broken link provides additional flexibility in the system design: $\kappa_G = \lambda/\lambda^{\rm St} > 1$ minimizes both the activation barriers and the reaction free energy lost in near-activationless electron transfer. The discontinuous ergodicity breaking makes some components of the phase space unavailable on the observation time $\tau_{\rm obs}$. For proteins, these inaccessible components are conformational states separated by high barriers, which cannot be overcome on the time $\tau_{\rm obs}$. Small changes of the thermodynamic state or low-energy alterations of the protein structure (e.g., ligand binding) typically would not allow access to those inaccessible components. On the contrary, continuous ergodicity breaking allows fine-tuning of the protein operation by constraining the phase space already available to the protein. It introduces the set of parameters $k\tau_j$ as additional control variables affecting statistical averages involved. Efficient control then requires a broad range of the relaxation times τ_j. This is the point at which the interfacial character of molecular biophysics becomes essential.

Interfaces break isotropy of the bulk and introduce uncompensated forces acting on the interfacial molecules. The interface responds to the force imbalance by creating significant gradients of the interfacial properties, such as the density gradient. These interfacial gradients drive long-wavelength collective deformations. Capillary waves at the liquid-gas interface is a classical example. A similar phenomenology applies to hydrated macromolecules. A folded protein finds itself in a shallow minimum formed by the competition between the attractions holding the residues in the close-packed folded structure and the puling force of hydrating water. The shallow character of the resulting minimum shows itself in large-scale fluctuations of the protein's total energy, on the scale of ~ 38 kcal/mol for a typical globular protein [106]. A large density of low-frequency normal modes, due to low rigidity of the folded polymer, leads to elastic deformations of the global protein shape and corresponding displacements of the charged surface residues. One arrives at the picture of electro-elastic fluctuations of the protein-water interface responsible for a significant breadth of electrostatic fluctuations recorded by catalytic sites. These intense electrostatic fluctuations, spreading many orders in magnitude in relaxation times, make continuous ergodicity breaking an efficient tool for tuning the energetics. To summarize, a number of very specific properties of proteins make them a special case, a "fluctuation machine", in the general phenomenology of electron-transfer reactions in condensed media. The main reason for this special status is the protein-water interface combining a large density of protein's charged residues, a sufficiently high elastic flexibility of the protein's outer layer, and highly polar water solvent polarized into dipolar domains.

There is obviously nothing specific to electron transport enzymes in the combination of two principles combined in their operation: (i) dynamical constrains on statistical averages and (ii) large-scale low-frequency fluctuations of the interface. The coupling

of the interfacial fluctuations to electrostatics (electro-elastic fluctuations) is significant for all processes requiring transferring charge, but will also affect any enzyme reaction involving polar reactants or with the alteration of polarity in the transition state.

The present discussion has mostly focused on the sub-ensemble of fast bath modes which contribute to the statistical averages on the reaction time-scale. The role of dynamically frozen variables has not been discussed and still requires better understanding. One, however, can note that dynamically frozen variables will contribute to fluctuations of electron-transport hopping sequences (rates of individual transitions) through the electron-transfer protein in each instance of one-electron cross-membrane transport. While one can consider the sequence of hops of a single electron as producing almost no entropy (low flux [11]), fluctuations of these hopping sequences, driven by the dynamically-frozen subset of variables, will contribute to the average work extracted from the enzyme and to the amount of entropy production (dissipation) [119].

A related issue is the problem of enzyme's aging. As electron moves in hops between the cofactors, the time elapsed from the injection of the electron into the chain allows the protein to explore more configurations consistent with the new charge state of the complex, including the existence of the positively charged substrate initiating the chain of electron hops (P^+ in figure 17 in the case of bacterial photosynthesis). The system ages in its thermodynamic state, as an ordinary glass does [14]. Periodic resetting of the enzyme to its initial configuration (thus bringing Sisyphus back to his rock [2]) is required to keep the consistency of operation. At the point of resetting, all the information content accumulated by the enzyme, including the information content involved in the dynamical restrictions, is dumped as an entropy release to the surroundings [123] (known as the Landauer principle [124, 125]). The system returns to its initial state to repeat the next cycle of operation.

This author has recently became aware of a not widely known article by Jaynes where the ideas discussed here were perhaps first anticipated. Quoting from Ref. [126]: "In a fast process, that happens in a time so short that thermal equilibrium of the whole system is never reached, only the phase volume belonging to those degrees of freedom actually involved in the interactions could be relevant; the second law may be applied in terms of Liouville's theorem in a relatively small subspace of the full one that we use in equilibrium theory." In terms of this article, nonergodic thermodynamics was offered by Jaynes as a general recipe for improving the efficiency of energy transduction in biology and a way to lift the requirement of increasing entropy imposed by the second law of thermodynamics on a spontaneous process in a closed dynamical system: "It is just to avoid thermalization that biological processes must take place rapidly, and thus we require a 'fast' second law to analyze them" [126]. When kinetic restrictions reduce the phase space from W to W_k, the only constraint imposed by the second law on the evolution of the system is that the phase volume does no shrink (Liouville's theorem) in any transition from the initial state "i" to the final state "f": $W_k^i \leq W_k^f$. Correspondingly, one gets for the entropy describing the restricted phase space $S_k^i \leq S_k^f$, in accord with the standard formulation of the second law. This requirement, however,

does not specify the thermodynamic entropies in the initial and final states: transitions of a closed system with a decrease of the thermodynamic entropy, $S^i > S^f$, are not prohibited. The standard requirement of the second law to increase the entropy of the enzyme and the bath is restored when the enzyme returns to the initial state and a new cycle begins.

Summarizing this historical account, penetrating insights by Monod [2] and Jaynes [126] formulated at the time when first data on energy transformation in biology were becoming available resonate with the new results nowadays produced by numerical sampling techniques. The new integration of biochemical pathways with statistical mechanics will require the combination of coarse-grained techniques based on information theory and the ensemble statistics far from equilibrium with microscopic mechanisms specifying the origins of fluctuations and collective modes driving enzymetic reactions.

Acknowledgments

This research is supported by the National Science Foundation (MCB-1157788). The author is grateful to John A. Venables (ASU) for triggering a re-connection between the restricted ensemble and Maxwell's demon and to Daniel R. Martin for reading the manuscript.

References

[1] N. Lane. *Power, Sex, Suicide. Mitochondria and the Meaning of Life*. Oxford University Press, Oxford, 2005.

[2] J. Monod. *Chance and Necessity: An Essay on the Natural Philosophy of Modern Biology*. Vintage Books, New York, 1971.

[3] D. G. Nicholls and S. J. Ferguson. *Bioenergetics 3*. Academic Press, London, 2002.

[4] R. A. Marcus and N. Sutin. Electron transfer in chemistry and biology. *Biochim. Biophys. Acta*, 811:265–322, 1985.

[5] P. F. Barbara, T. J. Meyer, and M. A. Ratner. Contemporary issues in electron transfer research. *J. Phys. Chem.*, 100:13148–13168, 1996.

[6] R. G. Compton and C. E. Banks. *Understanding Voltammetry*. World Scientific, Singapore, 2009.

[7] R. S. Knox and W. W. Parson. Entropy production and the Second Law in photosynthesis. *Biochim. Biophys. Acta - Bioenergetics*, 1767(10):1189–1193, 2007.

[8] R. E. Blankenship. *Molecular Mechanisms of Photosynthesis*. Blackwell Science, Williston, VT, 2003.

[9] A. J. Hoff and J. Deisenhofer. Photophysics of photosynthesis. *Phys. Rep.*, 287:1–247, 1997.

[10] R. A. Marcus. On the theory of oxidation-reduction reactions involving electron transfer. I. *J. Chem. Phys.*, 24:966, 1956.

[11] S. R. de Groot and P. Mazur. *Nonequilibrium Thermodynamics*. Dover, New York, 1984.

[12] P. M. Chaikin and T. C. Lubensky. *Principles of condensed matter physics*. Cambridge University Press, Cambridge, 1995.

[13] R. Kubo. Some aspects of the statistical-mechanical theory of irreversible processes. In *Lectures in Theoretical Physics*, volume 1, page 120. Interscience Publishers, Inc., New York, 1959.

[14] A. Crisanti and F. Ritort. Violation of the fluctuation–dissipation theorem in glassy systems: basic notions and the numerical evidence. *J. Phys. A: Math. Gen.*, 36:R181–290, 2003.
[15] R. G. Palmer. Broken ergodicity. *Adv. Phys.*, 31:669–735, 1982.
[16] C. A. Angell. Formation of glasses from liquids and biopolymers. *Science*, 267:1924–1935, 1995.
[17] H. Frauenfelder, G. Chen, J. Berendzen, P. W. Fenimore, H. Jansson, B. H. McMahon, I. R. Stroe, J. Swenson, and R. D. Young. A unified model of protein dynamics. *Proc. Natl. Acad. Sci.*, 106:5129–5134, 2009.
[18] M. Marconi, E. Cornicchi, G. Onori, and A. Paciaroni. Comparative study of protein dynamics in hydrated powders and in solution: A neutron scattering investigation. *Chem. Phys.*, 345:224–229, 2008.
[19] D. M. Leitner. Energy Flow in Proteins. *Ann. Rev. Phys. Chem.*, 59(1):233–259, 2008.
[20] S. Khodadadi and A. P. Sokolov. Protein dynamics: from rattling in a cage to structural relaxation. *Soft Matter*, 11(25):4984–4998, 2015.
[21] D. V. Matyushov. Nonergodic activated kinetics in polar media. *J. Chem. Phys.*, 130:164522, 2009.
[22] D. V. Matyushov. Energetics of electron transfer reactions in soft condensed media. *Acc. Chem. Res.*, 40:294–301, 2007.
[23] B. Peters. Common Features of Extraordinary Rate Theories. *J. Phys. Chem. B*, 119(21):6349–6356, 2015.
[24] I. Bahar, T. R. Lezon, L.-W. Yang, and E. Eyal. Global dynamics of proteins: Bridging between structure and function. *Ann. Rev. Biophys.*, 39:23–42, 2010.
[25] C. W. Gardiner. *Handbook of Stochastic Methods*. Springer, Berlin, 1997.
[26] B. J. Berne and R. Pecora. *Dynamic Light Scattering*. Dover Publications, Inc., Mineola, N.Y., 2000.
[27] J. P. Hansen and I. R. McDonald. *Theory of Simple Liquids*. Academic Press, Amsterdam, 2003.
[28] A. Migliore, N. F. Polizzi, M. J. Therien, and D. N. Beratan. Biochemistry and Theory of Proton-Coupled Electron Transfer. *Chem. Rev.*, 114(7):3381–3465, 2014.
[29] D. V. Matyushov. A phenomenological model of electron transfer in solvents near the glass-transition. *J. Chem. Phys.*, 122:084507, 2005.
[30] A. Nitzan. *Chemical Dynamics in Condensed Phases: Relaxation, Transfer and Reactions in Condensed Molecular Systems*. Oxford University Press, Oxford, 2006.
[31] M. Lax. The Frank-Condon principle and its application to crystals. *J. Chem. Phys.*, 20:1752–1760, 1952.
[32] A. Warshel. Dynamics of reactions in polar solvents. Semiclassical trajectory studies of electron-transfer and proton-transfer reactions. *J. Phys. Chem.*, 86(12):2218–2224, 1982.
[33] H. B. Gray and J. R. Winkler. Long-range electron transfer. *Proc. Natl. Acad. Sci.*, 102:3534–3539, 2005.
[34] S. S. Skourtis, D. H. Waldeck, and D. N. Beratan. Fluctuations in biological and bioinspired electron-transfer reactions. *Annu. Rev. Phys. Chem.*, 61(1):461–485, 2010.
[35] D. Noy, C. C. Moser, and P. L. Dutton. Design and engineering of photosynthetic light-harvesting and electron transfer using length, time, and energy scales. *Biochim. Biophys. Acta*, 1757:90–105, 2006.
[36] C. H. Bennett. Efficient estimation of free energy differences from Monte Carlo data. *J. Comput. Phys.*, 22(2):245–268, 1976.
[37] M. Tachiya. Relation between the electron-transfer rate and the free energy change of reaction. *J. Phys. Chem.*, 93(20):7050–7052, 1989.
[38] L. Reynolds, J. A. Gardecki, S. J. V. Frankland, and M. Maroncelli. Dipole solvation in nondipolar solvents: Experimental studies of reorganization energies and solvation dynamics. *J. Phys. Chem.*, 100:10337–10354, 1996.
[39] I. R. Gould, D. Noukakis, L. Gomes-Jahn, R. H. Young, J. L. Goodman, and S. Farid. Radiative and nonradiative electron transfer in contact radical-ion pairs. *Chem. Phys.*, 176:439–456,

1993.

[40] D. N. LeBard, D. R. Martin, S. Lin, N. W. Woodbury, and D. V. Matyushov. Protein dynamics to optimize and control bacterial photosynthesis. *Chem. Sci.*, 4:4127—4136, 2013.

[41] N. Ito, K. Duvvuri, D. V. Matyushov, and R. Richert. Solvent response and dielectric relaxation in supercooled butyronitrile. *J. Chem. Phys.*, 125:024504, 2006.

[42] D. V. Matyushov. Nanosecond Stokes shift dynamics, dynamical transition, and gigantic reorganization energy of hydrated heme proteins. *J. Phys. Chem. B*, 115:10715–10724, 2011.

[43] W. Doster. The protein-solvent glass transition. *Biochim. Biophys. Acta*, 1804:3–14, 2010.

[44] D. R. Martin and D. V. Matyushov. Microsecond dynamics of the protein and water affect electron transfer in a bacterial bc_1 complex. *J. Chem. Phys.*, 142:161101, 2015.

[45] P. G. Debenedetti and F. H. Stillinger. Supercooled liquids and glass transitions. *Nature*, 410:259, 2001.

[46] D. Kern, B.F. Volkman, P. Luginbühl, M. J. Nohaile, S. Kustu, and D. E. Wemmer. Structure of a transiently phosphorylated switch in bacterial signal transduction. *Nature*, 402:894–897, 1999.

[47] D. N. LeBard and D. V. Matyushov. Protein-water electrostatics and principles of bioenergetics. *Phys. Chem. Chem. Phys.*, 12:15335–15348, 2010.

[48] D. V. Matyushov. Protein electron transfer: Dynamics and statistics. *J. Chem. Phys.*, 139:025102, 2013.

[49] P. G. Wolynes, J. N. Onuchic, and D. Thirumalai. Navigating the folding routes. *Science*, 267:1619–1620, 1995.

[50] C. A. Angell. Insights into phases of liquid water from study of its unusual glass-forming properties. *Science*, 319:582 – 587, 2008.

[51] D. Thirumalai, Edward P. O'Brien, Greg Morrison, and Changbong Hyeon. Theoretical perspectives on protein folding. *Annu. Rev. Biophys.*, 39:159–183, 2010.

[52] S. C. L. Kamerlin and A. Warshel. At the dawn of the 21st century: Is dynamics the missing link for understanding enzyme catalysis? *Proteins*, 78:1339—1375, 2010.

[53] Andrew J. Adamczyk, Jie Cao, Shina C. L. Kamerlin, and Arieh Warshel. Catalysis by dihydrofolate reductase and other enzymes arises from electrostatic preorganization, not conformational motions. *Proc. Natl. Acad. Sci. U.S.A.*, 108(34):14115–14120, 2011.

[54] K. Henzler-Wildman and D. Kern. Dynamic personalities of proteins. *Nature*, 450:964–972, 2007.

[55] K. A. Henzler-Wildman, V. Thai, M. Lei, M. Ott, M. Wolf-Watz, T. Fenn, E. Pozharski, M. A. Wilson, G. A. Petsko, M. Karplus, C. G. Hubner, and D. Kern. Intrinsic motions along an enzymatic reaction trajectory. *Nature*, 450(7171):838–844, 2007.

[56] H. Eyring, S. H. Lin, and S. M. Lin. *Basic Chemical Kinetics*. Wiley-Interscience, New York, 1980.

[57] H.A. Kramers. Brownian motion in a field of force and the diffusion model of chemical reactions. *Physica*, 7(4):284–304, 1940.

[58] L. D. Zusman. Outer-sphere electron transfer in polar solvents. *Chem. Phys.*, 49:295–304, 1980.

[59] H. Sumi and R. A. Marcus. Dynamical effects in electron transfer reactions. *J. Chem. Phys*, 84:4894–4914, 1986.

[60] I. Rips and J. Jortner. Dynamic solvent effects on outer-sphere electron transfer. *J. Chem. Phys.*, 87(4):2090–2104, 1987.

[61] G. C. Walker, E. Åkesson, A. E. Johnson, N. E. Levinger, and P. F. Barbara. Interplay of solvent motion and vibrational excitation in electron-transfer kinetics: experiment and theory. *J. Phys. Chem.*, 96:3728–3736, 1992.

[62] N. Gayathri and B. Bagchi. Quantum and non-markovian effects in the electron transfer reaction dynamics in the marcus inverted region. *J. Phys. Chem.*, 100:3056–3062, 1996.

[63] I. Tuñón, D. Laage, and J. T. Hynes. Are there dynamical effects in enzyme catalysis? Some thoughts concerning the enzymatic chemical step. *Arch. Biochem. Biophys.*, page dx.doi.org/10.1016/j.abb.2015.06.004, 2015.

[64] L. D. Landau and E. M. Lifshits. *Statistical Physics*. Pergamon Press, New York, 1980.

[65] D. N. LeBard, V. Kapko, and D. V. Matyushov. Energetics and kinetics of primary charge separation in bacterial photosynthesis. *J. Phys. Chem. B*, 112:10322–10342, 2008.

[66] S. S. Skourtis. Probing protein electron transfer mechanisms from the molecular to the cellular length scales. *Biopolymers*, 100(1):82–92, 2013.

[67] G. N. Phillips and B. M. Pettitt. Structure and dynamics of the water around myoglobin. *Prot. Sci.*, 4(2):149–158, 1995.

[68] P. Ball. Water as an active constituent in cell biology. *Chem. Rev.*, 108:74, 2008.

[69] J. Spitzer and B. Poolman. How crowded is the prokaryotic cytoplasm? *FEBS Letters*, 587(14):2094–2098, July 2013.

[70] A. B. Fulton. How Crowded Is the Cytoplasm? Minireviews. *Cell*, 30:345–347, 1982.

[71] J.-M. Zanotti, M.-C. Bellissent-Funel, and J. Parello. Hydration-Coupled Dynamics in Proteins Studied by Neutron Scattering and NMR: The Case of the Typical EF-Hand Calcium-Binding Parvalbumin. *Biophys. J.*, 76(5):2390–2411, 1999.

[72] L. Hong, X. Cheng, D. Glass, and J. Smith. Surface Hydration Amplifies Single-Well Protein Atom Diffusion Propagating into the Macromolecular Core. *Phys. Rev. Lett.*, 108(23):238102, 2012.

[73] D. N. LeBard and D. V. Matyushov. Ferroelectric hydration shells around proteins: Electrostatics of the protein-water interface. *J. Phys. Chem. B*, 114:9246–9258, 2010.

[74] D. R. Martin and D. V. Matyushov. Dipolar nanodomains in protein hydration shells. *J. Phys. Chem. Lett.*, 6(3):407–412, 2015.

[75] D. I. Svergun, S. Richard, M. H. J. Koch, Z. Sayers, S. Kuprin, and G. Zaccai. Protein hydration in solution: Experimental observation by x-ray and neutron scattering. *Proc. Natl. Acad. Sci.*, 95:2267–2272, 1998.

[76] F. Pizzitutti, M. Marchi, F. Sterpone, and P. J. Rossky. How protein surfaces induce anomalous dynamics of hydration water. *J. Phys. Chem. B*, 111(26):7584–7590, 2007.

[77] D. V. Matyushov. Dipolar response of hydrated proteins. *J. Chem. Phys.*, 136:085102, 2012.

[78] M. Heyden, D. J. Tobias, and D. V. Matyushov. Terahertz absorption by dilute aqueous solutions. *J. Chem. Phys.*, 137:235103, 2012.

[79] D. R. Martin and D. V. Matyushov. Hydration shells of proteins probed by depolarized light scattering and dielectric spectroscopy: Orientational structure is significant, positional structure is not. *J. Chem. Phys.*, 141:22D501, 2014.

[80] S. Sarupria and S. Garde. Quantifying water density fluctuations and compressibility of hydration shells of hydrophobic solutes and proteins. *Phys. Rev. Lett.*, 103:037803, 2009.

[81] D. N. LeBard and D. V. Matyushov. Dynamical transition, hydrophobic interface, and the temperature dependence of electrostatic fluctuations in proteins. *Phys. Rev. E*, 78:061901, 2008.

[82] G. Schirò, M. Fomina, and A. Cupane. Communication: Protein dynamical transition vs. liquid-liquid phase transition in protein hydration water. *J. Chem. Phys.*, 139(12):121102, 2013.

[83] G. A. Samara. The relaxational properties of compositionally disordered abo_3 porovsketes. *J. Phys.: Condens. Matter*, 15:R367–R411, 2003.

[84] D. J. Barlow and J. M. Thornton. Charge distribution in proteins. *Biopolymers*, 25:1717–1733, 1986.

[85] R. A. Marcus. Electron transfer reactions in chemistry. Theory and experiment. *Rev. Mod. Phys.*, 65:599, 1993.

[86] C. G. Gray and K. E. Gubbins. *Theory of Molecular Liquids*. Clarendon Press, Oxford, 1984.

[87] D. V. Matyushov and R. Schmid. Optical and radiationless intramolecular electron transitions in nonpolar fluids: Relative effects of induction and dispersion interactions. *J. Chem. Phys.*, 103:2034–2049, 1995.

[88] J. D. Jackson. *Classical Electrodynamics*. Wiley, New York, 1999.

[89] A. A. Milischuk and D. V. Matyushov. Quadrupolar solvatochromism: 4-amino-phthalimide in

toluene. *J. Chem. Phys.*, 124:204502, 2006.

[90] D. V. Matyushov. Solvent reorganization energy of electron transfer in polar solvents. *J. Chem. Phys.*, 120:7532–7556, 2004.

[91] D. Borgis, L. Gendre, and R. Ramirez. Molecular Density Functional Theory: Application to Solvation and Electron-Transfer Thermodynamics in Polar Solvents. *J. Phys. Chem. B*, 116(8):2504–2512, 2012.

[92] L. D. Landau and E. M. Lifshitz. *Electrodynamics of Continuous Media*. Pergamon, Oxford, 1984.

[93] L. Onsager. Electric moments of molecules in liquids. *J. Am. Chem. Soc.*, 58:1486–1493, 1936.

[94] F. Tama and C. L. Brooks. Symmetry, form, and shape: Guiding principles for robustness in macromolecular machines. *Annu. Rev. Biophys. Biomol. Struct.*, 35:115–133, 2006.

[95] D. R. Martin and D. V. Matyushov. Solvent-renormalized dissipative electro-elastic network model of hydrated proteins. *J. Chem. Phys.*, 137:165101, 2012.

[96] D. R. Martin and D. V. Matyushov. Non-Gaussian statistics and nanosecond dynamics of electrostatic fluctuations affecting optical transitions in a green fluorescent protein. *J. Phys. Chem. B*, 116:10294–10300, 2012.

[97] J. Blumberger and M. Sprik. Quantum vs classical electron transfer energy as reaction coordinate for the aqueous Ru^{2+}/Ru^{3+} redox reaction. *Theor. Chem. Acc.*, 115:113–126, 2006.

[98] W. Doster. The dynamical transition of proteins, concepts and misconceptions. *Eur. Biophys. J.*, 37:591, 2008.

[99] R. Richert and A. C. Angell. Dynamics of glass-forming liquids. V. On the link between molecular dynamics and configuration entropy. *J. Chem. Phys.*, 108:9016, 1998.

[100] A. Warshel. Dynamics of reactions in polar solvents. Semiclassical trajectory studies of electron-transfer and proton-transfer reactions. *J. Phys. Chem.*, 86:2218–2224, 1982.

[101] J. K. Hwang and A. Warshel. Microscopic examination of free-energy relationships for electron transfer in polar solvents. *J. Am. Chem. Soc.*, 109(3):715–720, 1987.

[102] R. A. Kuharski, J. S. Bader, D. Chandler, M. Sprik, M. L. Klein, and R. W. Impey. Molecular model for aqueous ferrous-ferric electron transfer. *J. Chem. Phys.*, 89:3248–3257, 1988.

[103] M. Tachiya. Effect of the dielectric saturation on the rates of electron transfer in polar solvents. *Chem. Phys. Lett.*, 159:505, 1989.

[104] D. V. Matyushov and G. A. Voth. Modeling the free energy surfaces of electron transfer in condensed phases. *J. Chem. Phys.*, 113:5413, 2000.

[105] V. Tipmanee, H. Oberhofer, M. Park, K. S. Kim, and J. Blumberger. Prediction of Reorganization Free Energies for Biological Electron Transfer: A Comparative Study of Ru-Modified Cytochromes and a 4-Helix Bundle Protein. *J. Am. Chem. Soc.*, 132(47):17032–17040, 2010.

[106] A. Cooper. Protein fluctuations and the thermodynamic uncertainty principle. *Prog. Biophys. Molec. Biol.*, 44(3):181–214, 1984.

[107] S. Mukamel. *Principles of Nonlinear Optical Spectroscopy*. Oxford University Press, New York, 1995.

[108] D. N. LeBard and D. V. Matyushov. Energetics of bacterial photosynthesis. *J. Phys. Chem. B*, 113:12424–12437, 2009.

[109] H. Wang, S. Lin, J. P. Allen, J. C. Williams, S. Blankert, C. Laser, and N. W. Woodbury. Protein dynamics control the kinetics of initial electron transfer in photosynthesis. *Science*, 316:747–750, 2007.

[110] J. Kraut. How do enzymes work? *Science*, 242(4878):533–540, 1988.

[111] P. A. Srere. Why are enzymes so big? *Trends Biochem. Sci.*, 9(9):387–390, 1984.

[112] A. Cooper and D. T. F. Dryden. Allostery without conformational change. *Eur. Biophys. J.*, 11(2):103–109, 1984.

[113] A. W. Fenton. Allostery: an illustrated definition for the 'second secret of life'. *Trends in Biochem. Sci.*, 33(9):420–425, 2008.

[114] H. N. Motlagh, J. O. Wrabl, J. Li, and V. J. Hilser. The ensemble nature of allostery. *Nature*,

508(7496):331–339, April 2014.

[115] S. K. Pal and A. H. Zewail. Dynamics of water in biological recognition. *Chem. Rev.*, 104:2099–2123, 2004.

[116] A. Warshel, P. K. Sharma, M. Kato, and W. W. Parson. Modeling electrostatic effects in proteins. *Biochim. Biophys. Acta*, 1764:1647–1676, 2006.

[117] D. R. Martin and D. V. Matyushov. Photosynthetic diode: Electron transport rectification by wetting the quinone cofactor. *Phys. Chem. Chem. Phys.*, page DOI: 10.1039/c5cp03397g, 2015.

[118] C. Beck and F. Schlögl. *Thermodynamics of chaotic systems*. Cambridge University Press, Cambridge, 1993.

[119] J. M. R. Parrondo, J. M. Horowitz, and T. Sagawa. Thermodynamics of information. *Nat. Phys.*, 11(2):131–139, 2015.

[120] H. S. Leff and A. F. Rex. Overview. In *Maxwell's demon. Entropy, Information, Computing*. Princeton University Press, New Jersey, 1990.

[121] E. T. Jaynes. Gibbs vs Boltzmann Entropies. *Am. J. Phys.*, 33(5):391–398, 1965.

[122] A. C. Elitzur. Let there be life. *J. Theor. Biol.*, 168:429–459, 1994.

[123] C. H. Bennett. The thermodynamics of computation - a review. *Int. J. Theor. Phys.*, 21(12):905–940, 1982.

[124] R. Landauer. Irreversibility and the heat generation in the computing process. *IBM J. Res. Dev.*, 5(3):183–191, 1961.

[125] M. Esposito and C. Van den Broeck. Second law and Landauer principle far from equilibrium. *Europhys. Lett.*, 95(4):40004, 08.

[126] E. T. Jaynes. Cleaning up mysteries – the original goal. In J. Skilling, editor, *Maximum Entropy and Bayesian Methods*, pages 1–27, Dordrecht, Holland, 1989. Kluwer Academic Press.